

Chapter - 4

Photoluminescence of

Strontium

Pyrophosphate

4.1. Introduction

In this chapter, the basic information of photoluminescence (PL) is described in detail. The principle of photoluminescence, theoretical background, and PL mechanism, instrumentation of PL spectrometer, applications of phosphor, etc are explained briefly. The chapter contains some significant experimental results and discussion of photoluminescence property of rare earth doped strontium pyrophosphate. The outcome of PL results has been discussed on the basis of theory and its application in detail.

4.2. Photoluminescence

4.2.1. Overview

The luminescent materials are generally called as phosphors that emit light when it is excited by radiation. Majority phosphors consisting of solid inorganic polycrystalline powder materials [1]. The phosphors mainly consisting of a host lattice and a small fraction of intentionally doped impurity ions [1, 2]. Generally, the percentage concentrations of impurity ions are taken low, because of the luminescence yield decreases at higher concentrations due to the concentration quenching [1-3]. The absorption of incident radiation energy is taken place by the host lattice or by the impurity ion [4, 5]. In the major luminescence process, the exciting radiation energy absorbed by the doped impurity ions also called as an activator, raising it to the excited state. The excited state can return to the ground state by the emission of visible radiation [6]. In some cases, when the activator ions are not capable of absorption radiation, another type of impurity ions can be added called as sensitizers. The sensitizer ions can absorb the radiation energy and consequently transfer this energy to the activator ions to raising it to excited state [2, 7]. In this type of process, the energy transport phenomenon has been involved through luminescent materials. The range of emission wavelength can be adjusted by selecting the appropriate impurity ions or a combination of impurity ions in the same host lattice [2, 6]. Some trivalent rare earth activator ions show their characteristic emission spectra which cannot be affected by the chemical environment of the host lattice.

4.2.2. Principle

Photoluminescence (PL) is the spontaneous emission of light from the material under optical excitation by UV, visible or infrared radiation. Photoluminescence process that takes place in any fluorimetry analysis [8]. The absorption of UV, visible or infrared

regions of the spectrum cause the excitation of the outer most orbital electrons of the atom or molecule which can very useful interest in fluorimetry [9]. Classification of luminescence phenomenon is firmly based on the electronic configuration of the material in which provide the excited state and the emission path to electron [10-12]. Luminescence process is divided into two class, fluorescence and phosphorescence. Generally, in fluorescence process, the emission of light occurs fast because within the time period of the order of nanosecond while in phosphorescence process the emission of light takes place slowly in the time period of the order of microsecond to hours or even days [12]. Photoluminescence (PL) phenomenon also categorized on the basis of large-scale inorganic materials that generally revealing phosphorescence, as well as the smaller organic dye molecules and inorganic nano-materials, which can reveal either fluoresce or phosphoresce [13].

4.2.3. Photoluminescence Mechanism

In the photoluminescence phenomenon, the mechanism of excitation and emission processes have been classically represented by the Polish physicist Prof. Alexander Jablonski through the Jablonski energy level diagram as shown in Figure 4.1. At room temperature, the atoms or molecules can generally occupy the lowest vibrational energy level of the ground state to attain its stability [14, 15]. After the absorption of radiation, atoms or molecules are raised to the excited states. As shown in Figure 4.1, the absorption of radiation energy by the atom or molecules of the phosphor can elevate the ground state electrons to the either in the first excited state S_1 or second excited state S_2 . There are different energy levels involved in the excitation and emission process of light [16-18].

In Jablonski diagram, S_0 is the singlet ground state, and S_1 and S_2 be the first and second excited singlet states which are aligned in a stack formation as horizontal lines. The lowest energy level line in each state denotes the electronic energy levels, and the other higher order lines represent the different vibrational energy levels [19-21]. Symbolic representation of different transitions is demonstrated in Figure 4.1.

The emission of light from the phosphors can occur through three important processes, which can take place at different timescales. Several orders of the magnitude of time scale [22, 23] are given in Table 4.1. In the first process, after the absorption of radiation energy, the excitation of the molecule due to the incoming photon can occur in femtoseconds. In the second process, the vibrational nonradiative relaxation of excited

electrons to the lowest energy level can take place in picoseconds [24-26]. The third process, the emission of a longer wavelength or low energy photon through the return of the excited molecule to the ground state can occur after a long time period of the order of nanoseconds [27, 28]. There are some other processes such as internal conversion, intersystem crossing, non-radiative relaxation quenching also take place at different order timescale which is given in Table 4.1.

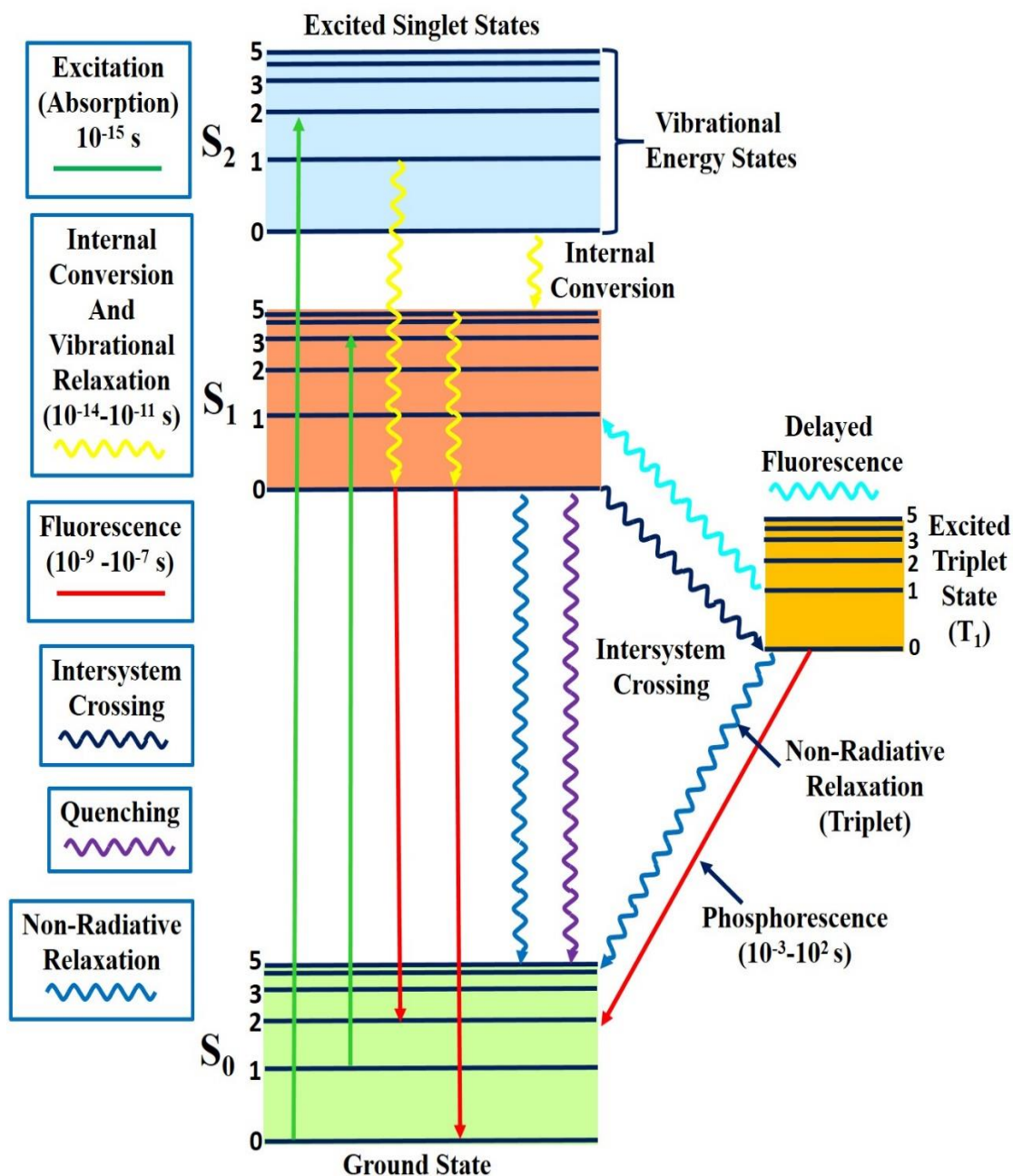


Figure 4.1 Jablonski energy level diagram for the photoluminescence mechanism.

Transition	Process	Rate Constant	Timescale (s)
$S_0 \rightarrow S_1$ or S_n	Absorption (Excitation)	Instantaneous	10^{-15}
$S_n \rightarrow S_1$	Internal Conversion	$k(I_C)$	10^{-14} to 10^{-10}
$S_1 \rightarrow S_1$	Vibrational Relaxation	$k(V_R)$	10^{-12} to 10^{-10}
$S_1 \rightarrow S_0$	Fluorescence	$k(F)$	10^{-9} to 10^{-7}
$S_1 \rightarrow T_1$	Intersystem Crossing	$k(pT)$	10^{-10} to 10^{-8}
$S_1 \rightarrow S_0$	Non-Radiative Relaxation Quenching	$k(NR), k(Q)$	10^{-7} to 10^{-5}
$T_1 \rightarrow S_0$	Phosphorescence	$k(P)$	10^{-3} to 100
$T_1 \rightarrow S_0$	Non-Radiative Relaxation Quenching	$k(NR), k(QT)$	10^{-3} to 100

Table 4.1 Timescale range for fluorescence processes [21, 29, 30].

4.2.3.1. Absorption and Excitation

Absorption and excitation processes are taking in a very short interval of time in the phosphor. Generally phosphor irradiation with a wide range UV-Visible spectrum, that can excite a whole range of allowed electron transition. Therefore, the excited electrons populate the different vibrational energy levels of the excited states. Certain transitions out of these whole transitions have a very high degree of probability, which can constitute the absorption spectrum of the phosphor. In most of the phosphors, the absorption spectra and excitation spectra are different, but they can generally overlap on each other as well as occasionally indistinguishable. The majority of the phosphor can usually excited under the higher vibrational energy level of the first S_1 or second S_2 singlet energy state when it absorbs the UV or visible light photon [31, 32]. The excitation transition after absorption of such photon is shown in Figure 4.1. The first green arrow in upward direction represents the excitation transition occurs from the lowest vibrational energy level of the ground state to a third vibrational level in the second excited state ($S_0 = 0 \rightarrow S_2 = 3$) [33-35]. The second green arrow in upward direction represents the excitation transition occurs from the second vibrational level of the ground state to the fifth vibrational level in the first excited state ($S_0 = 0 \rightarrow S_1 = 5$) [36, 37]. The possibility of the transition taking place by the electron of the ground state S_0 to the excited first singlet state S_1 or second singlet state S_2 mainly depends on the selection rules follow by the vibrational and rotational energy states, as well as the energy of an electron is been present in the ground state to that of an electron present in the excited state [38]. The probability of the most preferential transition in which the electron

density of the rotational and vibrational energy level is overlap maximum in the ground state and excited states of the phosphor [39]. As a result, the incident light of variable wavelength has enough energy to be absorbed and often yield transitions that give rise the multiple peaks or broad absorption spectrum [40]. In phosphor, the wide-ranging photons from UV to IR with different energies associated with the absorption transitions and forming the broad band spectra rather than separate lines.

4.2.3.2. Emission

The excitation spectrum of the phosphor can be obtained by scanning the phosphor through a single wavelength having maximum emission intensity in emission spectra [41]. Another method to excite the phosphor by a single wavelength having maximum absorption intensity in excitation spectra. It can reveal the emission spectrum profile of the phosphor. The excitation spectra and emission spectra of the phosphor is the result of the probability distribution functions in which a photon of given quantum energy is absorbed and eventually allowed phosphor to emit a photon in the form of photoluminescence radiation [3, 20].

4.2.4. Instrumentation of Photo-spectrometer

The photoluminescence spectra of all phosphors were recorded through the Shimadzu RF-5301 spectrofluorophotometer where the phosphors were excited by 150 W xenon lamp used as excitation source. All PL spectra were recorded at Department of Applied Physics, Faculty of Technology, M. S. University of Baroda, Vadodara. Figure 4.2 shows PL instrument used for PL spectra measurements.

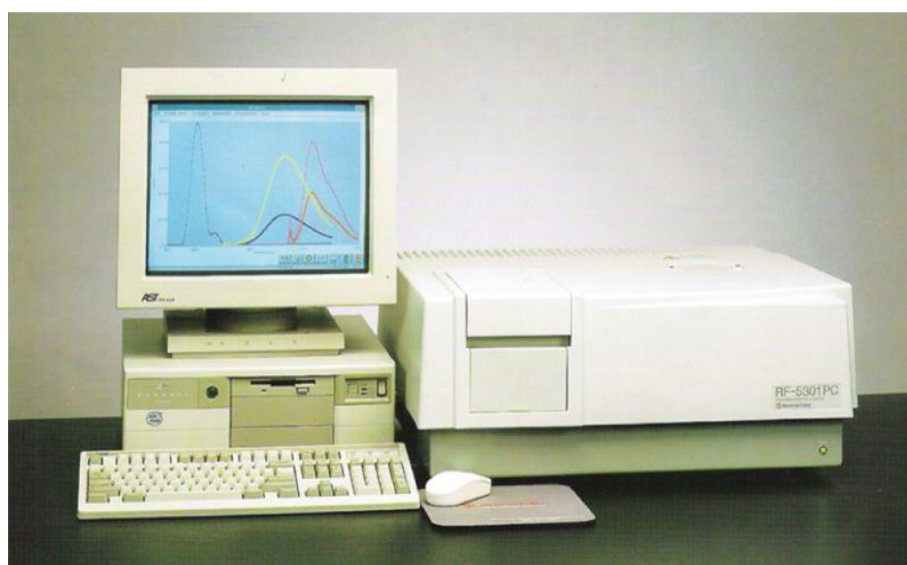


Figure 4.2 Shimadzu spectrofluorophotometer for PL measurements.

4.2.5. Applications

4.2.5.1. Light Emitting Diode (LED)

In recent time, white light-emitting diode (WLED) has been widely accepted as a green light source for the next generation that can replace conventional incandescence and fluorescence lamps [42]. Low power consumption, high efficiency, low cost, long lasting life and light free of mercury are the main advantages of LED light. The cost of WLED production could be high because white light could be generated by two or three complementary LED chips [43]. Therefore, the one wavelength LED converted phosphor is very useful to the economically cheap method to produce WLED.

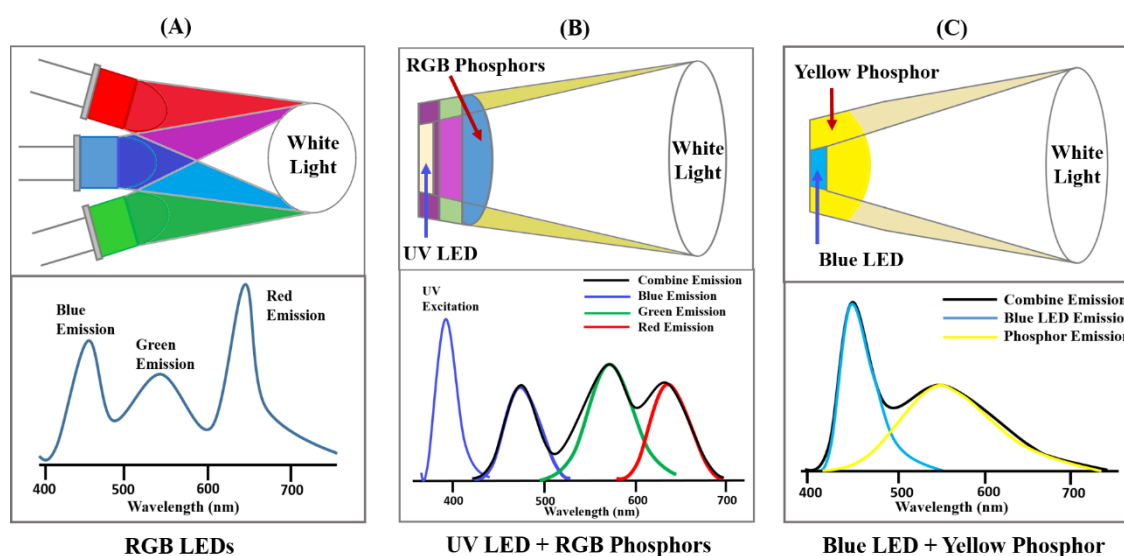


Figure 4.3 Three types of white LEDs manufactured by different methods; (A) Red + Green + Blue LEDs. (B) UV LED + RGB phosphor. (C) Blue LED + Yellow phosphor.

White LEDs can be manufactured through three different approaches as shown in Figure 4.3. In First method (As shown in Figure 4.3 (A)), the white light can obtain from three different monochromatic LED sources of red, blue and green (RGB) colors which are sensitive to the RGB sensors of human eyes [44]. This type of white LED having high production cost as well as the output white color is unstable because of the color degrade fast at different rates [45]. In the second method (As shown in Figure 4.3 (B)), the combination of UV LED and RGB phosphors are used to obtain white light, the perception similar to the fluorescent tubes such LED termed as RGB – LEDs. In such type of white LED, UV LED to pump a combination of red, green and blue light phosphors that can combine emit white light [46]. The main advantage of RGB – LED are that they deliver a white light that can have high efficiency and variable color point

[46]. In the third method (As shown in Figure 4.3 (C)), a blue LED and the yellow phosphor are used to obtain white light, in which blue LED is used to pump yellow phosphor integrated LED such type of LED termed as phosphor converted LED (pc-LED) [47]. The pc-LED blue light emitted from the blue LED is used to excite the yellow phosphor, during such process some part of blue light leak through the phosphor and combined form white light. The commercial production of white LEDs mainly base on the third method explained in Figure 4.3(C). In which the combination of a single blue light emitting LED chip ($\lambda_{\text{emission}} = 440 - 460 \text{ nm}$) with yellow phosphor ($\lambda_{\text{emission}} \approx 560 \text{ nm}$) i.e., Cerium doped Yttrium Aluminium Garnet (YAG: Ce). This pc-LEDs have a color rendering index (CRI) of 70 – 80 and a correlated color temperature (CCT) of 4000 – 8000 K which is suitable for outdoor applications and sensitive to the human eyes [44]. The low cost-performance merits and high efficiency of traditional incandescent bulbs are the main advantages of pc-LED.

4.2.5.2. Fluorescence Lamp

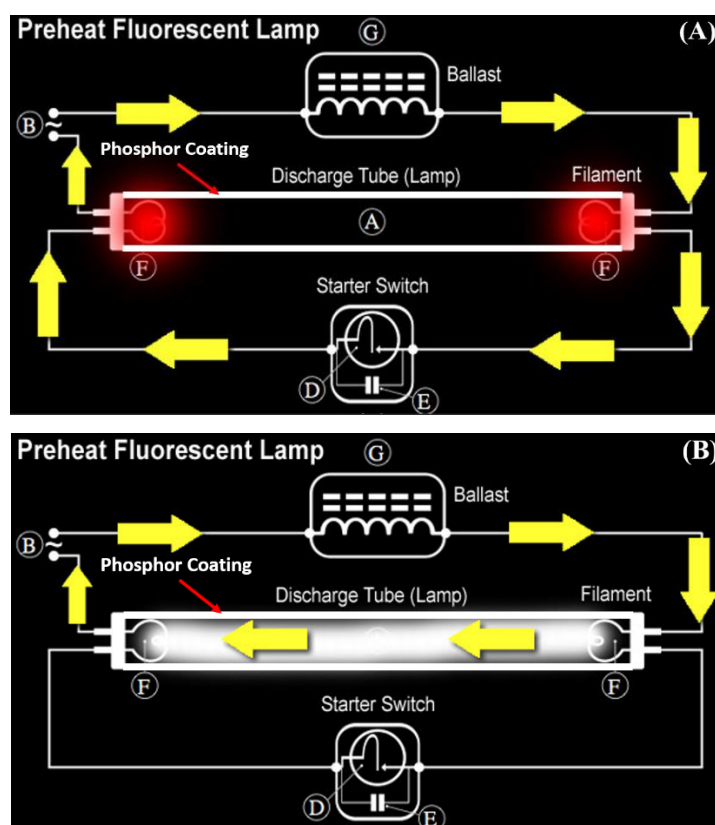


Figure 4.4 Working of fluorescence lamp; (A) Hg Discharge, (B) Emission of visible light.

The majority of luminescent materials are used by the lighting industry for the production of fluorescence lamps. In which the phosphors are mainly used for coating of

the inner surface of the fluorescence tube. In fluorescence lamp when a current passing through the filament of the lamp, the Hg get a discharge and produce UV light due to the electronic transition of Hg atoms [48]. At low pressure, the discharge of Hg produces UV light of the wavelength 254 nm. This high energetic UV light is used to excite the coated phosphors and emits the visible light [49]. The phosphors used for the application of fluorescence lamp should have strong absorption at 254 nm, as a result, the UV light efficiently converted into visible light [50]. Figure 4.4 shows the working of a fluorescence lamp.

4.2.5.3. Scintillator

Some phosphor has characteristics of emission of visible light when it is excited by the high energy ionizing radiation x-rays and gamma rays, such luminescent materials are termed as scintillators [51, 52]. Some glassy, plastic, inorganic and organic materials, as well as some liquids and gases, are used as scintillators in various fields like medical imaging, industrial inspections, security applications, and high-energy physics calorimetry and geophysical exploration [53-55]. The physical mechanism of scintillators are as follow: First is the absorption of the high energetic ionizing radiation due to the band structure of phosphor, Second is the absorption of radiation resulting in the transfer of electrons from the valence to conduction band of the material; Third is the transfer from the electron-hole recombination energy to the luminescent center; and fourth is the emission of visible light [55, 56]. The general requirements of scintillator phosphors are the fast response time up to 10–100 ns, high emission yield, high density, and high atomic number [57]. There are several rare earth doped polycrystalline bulk materials based on slow 4f-4f transitions of rare-earth ions which have been capable to detect high-energy rays [58].

4.2.5.4. Up-conversion Phosphor

The up-conversion phenomenon is one of the general cases in which one or more than one low energy photons are absorbed by the phosphor, and emit high energy photons [59]. The luminescent materials that are able to cause such type of effect are known as up-conversion phosphor. There exist different processes occurs in up-conversion phenomenon. The up-conversion process can be classified in two manners according to the physical mechanism involved in the occurrence of it: (i) single photon and (ii) multiphoton processes. [60, 61] The process in which one higher wavelength (lower energy) photon is absorbed during the excitation and subsequently emits a lower

wavelength (higher energy) photon, this process is termed as single photon conversion [62, 63]. Single photon conversion occurs due to anti-Stokes emission. In single photon conversion, the additional energy is been delivered by the host lattice in the form of the annihilation of one or more phonons [3, 64]. There are several processes are involved in the multi-photon conversion. In this processes, two or more incident lower energy photons absorbed during the excitation and are converted into one emitted photon of (substantially) higher energy [65, 66]. There are some different type of up-conversion process are described through the energy band diagram in Figure 4.5. In the figure, vertically upward arrows represent the absorption process, vertically downward arrows represent the emission process, dotted lines indicate non-radiative energy transfer processes and dashed horizontal lines indicate virtual states [50].

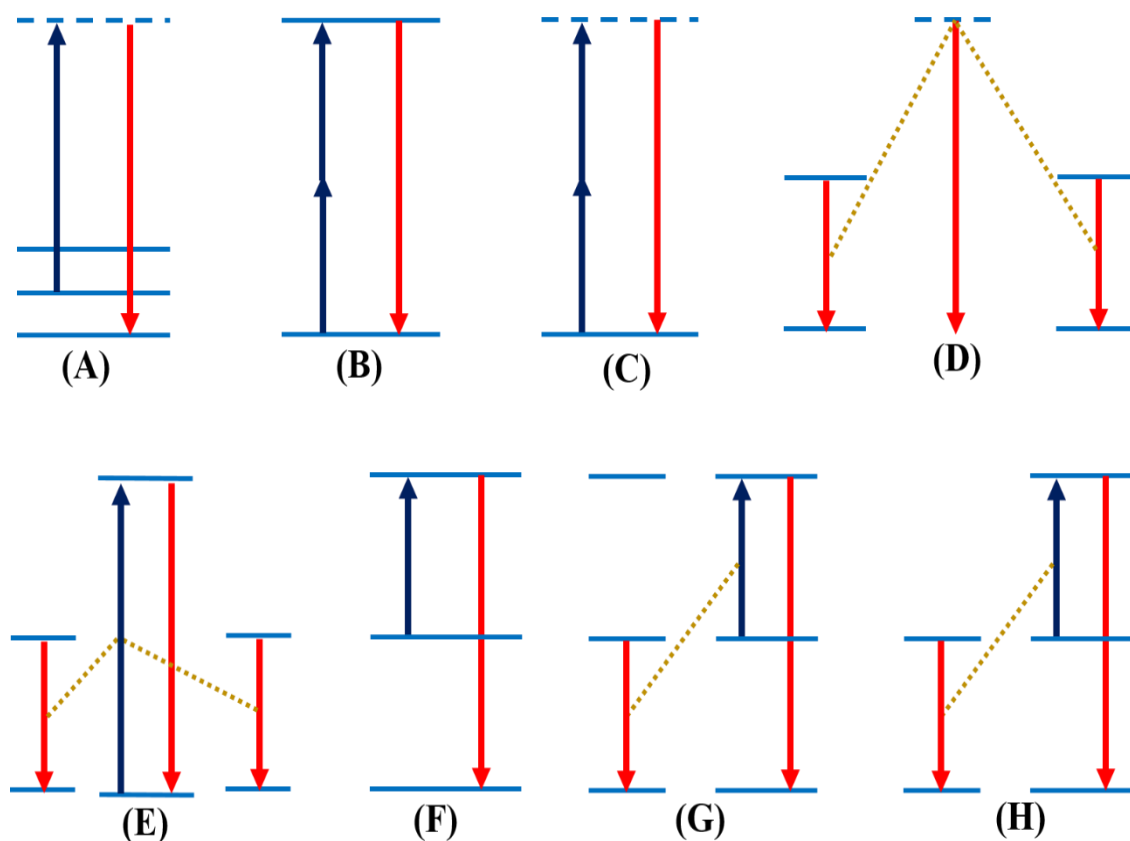


Figure 4.5 Eight of the most relevant up-conversion processes: (A) anti-Stokes Raman emission, (B) 2-photon excitation, (C) second harmonic generation, (D) cooperative luminescence, (E) cooperative sensitization, (F) excited state absorption, (G) energy transfer up-conversion, and (H) sensitized energy transfer up-conversion [50, 59].

4.3. Rare Earth Doped Strontium Pyrophosphate

The photoluminescence properties of RE^{3+} doped $\text{Sr}_2\text{P}_2\text{O}_7$ phosphors were studied for the different concentrations of dopant ions. For this study, 0.5- 5.0 mol% RE^{3+} (Ce^{3+} , Eu^{3+} , Tb^{3+} , Dy^{3+} , Er^{3+} , Gd^{3+}) doped $\text{Sr}_2\text{P}_2\text{O}_7$ phosphors were synthesized by combustion method at heating temperature 1200°C . For the PL measurements, the phosphors were excited under different emission wavelength, and corresponds to the excitation spectra of the phosphors emission spectra were recorded for different excitation wavelength.

4.3.1. $\text{Sr}_2\text{P}_2\text{O}_7: \text{Ce}^{3+}$

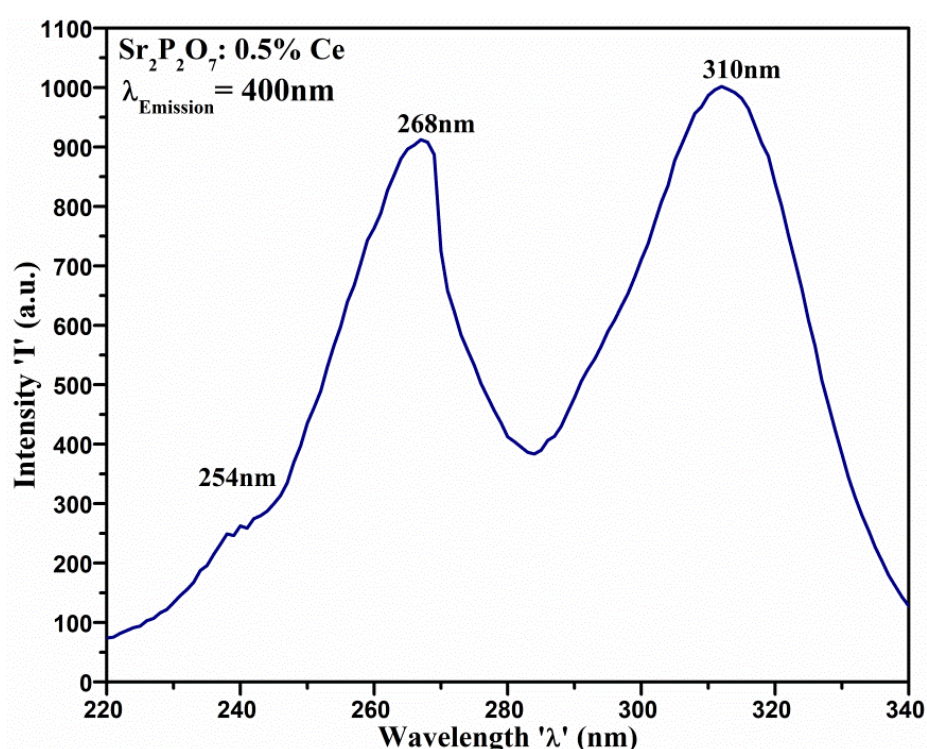


Figure 4.6 PL excitation spectra of Ce^{3+} doped $\text{Sr}_2\text{P}_2\text{O}_7$ phosphor.

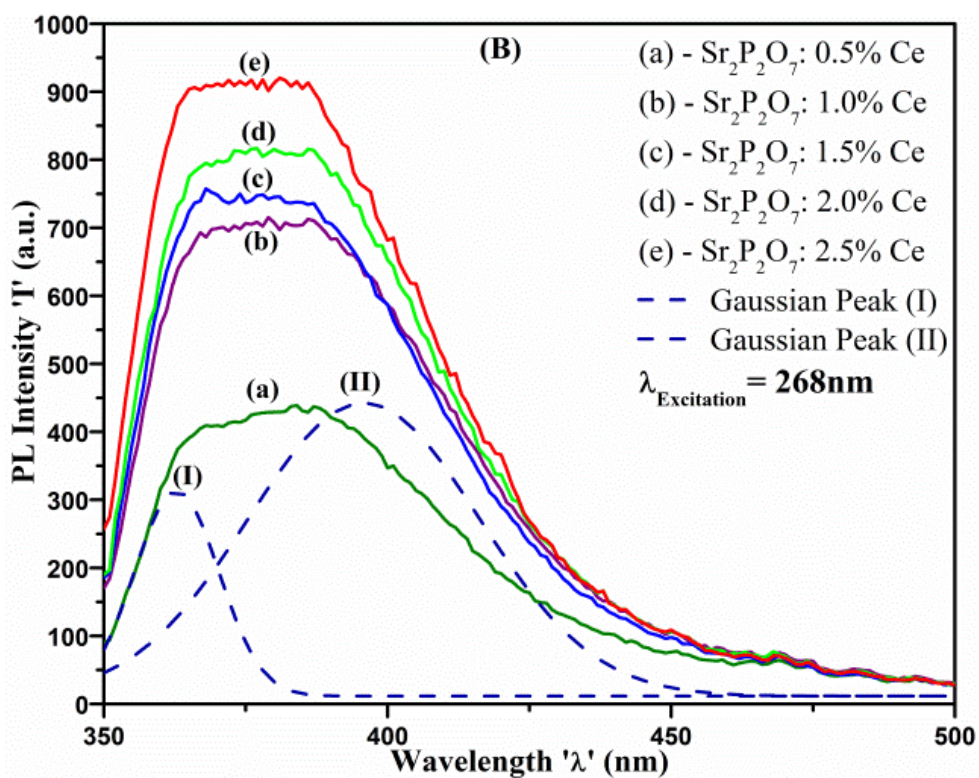
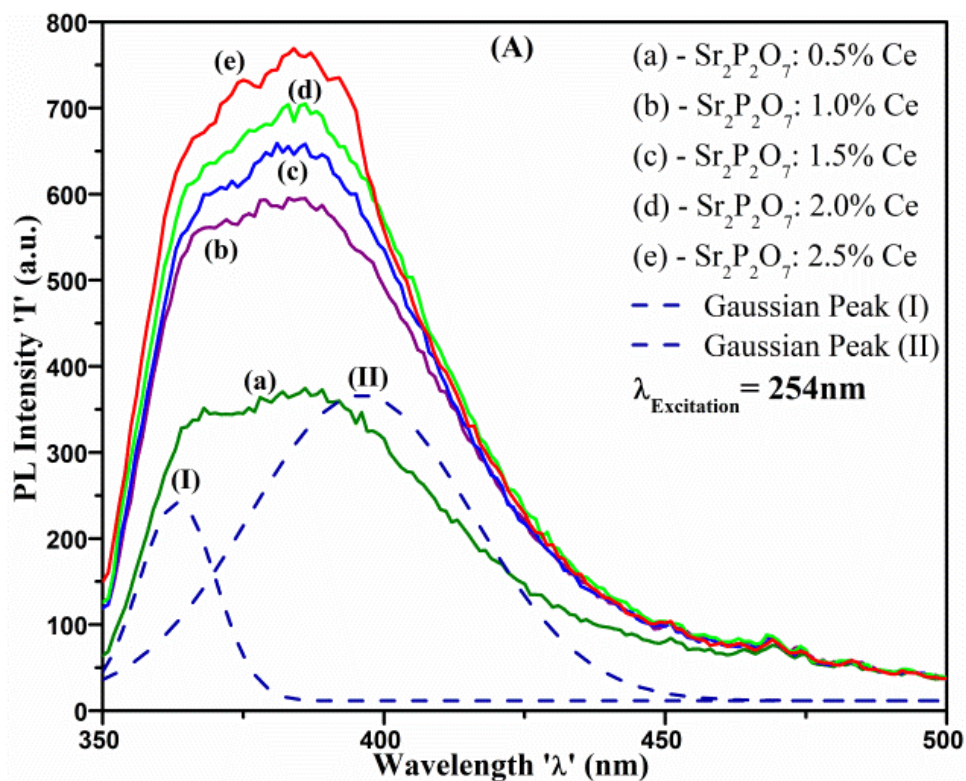
The PL excitation spectra of Ce^{3+} strontium pyrophosphate recorded at $\lambda_{\text{Emission}} = 400 \text{ nm}$ is shown in Figure 4.6. In excitation spectra, two broad excitation bands at 268 nm and 310 nm are ascribed to the $5d - 4f$ electronic transitions of Ce^{3+} in the host lattice. A shoulder peak at 254 nm at the beginning of the excitation spectra is ascribed due to the host absorption. The broad absorption band at 310 nm is attributed due to the allowed transition from the $^2\text{F}_{5/2}$ ground state to the lowest $5d$ state of Ce^{3+} located at the host lattice site of Sr^{2+} ion [67]. The weak absorption peak at 254 nm and the strong absorption band of host occurs at 268 nm, which corresponds due to the valance band to conduction

band inter-band transition of $\text{Sr}_2\text{P}_2\text{O}_7$ hosts. The strong broad absorption band shaped in the range of 282 – 340 nm might occur owing to the three closely lying bands correspond to the Ce^{3+} intra-ion $4f \rightarrow 5d(j)$ ($j = 1, 2, 3$) transitions. The geometric deviation of octahedra of Ce^{3+} ion in host lattice is not large enough to make $5d(j)$ ($j=1, 2, 3$) sub-levels well separated which is the reason for the occurrence of broad absorption centered at 310 nm.

PL emission spectra of $\text{Sr}_2\text{P}_2\text{O}_7: x \text{Ce}^{3+}$ ($x = 0.5, 1.0, 1.5, 2.0$ and 2.5 mol%) phosphors are recorded at excitation wavelength 254 nm, 268 nm and 310 nm are shown in Figure 4.7 (A), (B) and (C), respectively. $\text{Sr}_2\text{P}_2\text{O}_7: x\% \text{Ce}^{3+}$ phosphor exhibits high-intensity emission band centered at around 385 nm under the multiple excitations. The emission band of Ce^{3+} doped $\text{Sr}_2\text{P}_2\text{O}_7$ powder samples is revealed the typical characteristic emission of Ce^{3+} ion in the range of 350 – 450 nm. Gaussian curve fitting of the PL emission spectra of the Ce^{3+} – doped $\text{Sr}_2\text{P}_2\text{O}_7$ phosphor revealed that the emission originates from the $5d$ – the $4f$ transition of Ce^{3+} . PL emission spectrum of $\text{Sr}_2\text{P}_2\text{O}_7$ phosphor for different excitation wavelength consists of two Gaussian peaks at 363 nm and 395 nm. The observed doublet Gaussian bands in the near-UV range are due to the allowed transitions of Ce^{3+} ions from the relaxed lowest $5d$ excited state to the $^2\text{F}_{5/2}$ and $^2\text{F}_{7/2}$ ground states [67]. The $4f^1$ ground state yields two levels of $^2\text{F}_{5/2}$ and $^2\text{F}_{7/2}$ due to the spin-orbit coupling of $4f$ state. The energy discrepancy between the two Gaussian bands, the first situated at 363 nm ($27,397 \text{ cm}^{-1}$) and the second at 395 nm ($25,316 \text{ cm}^{-1}$) is about 2081 cm^{-1} [68]. The Gaussian peak-fitting results of PL emission band of Ce^{3+} doped suggest Ce^{3+} ion $4f$ level L–S splitting value is 2081 cm^{-1} , which is near to the familiar value of 2000 cm^{-1} in the literature [69, 70].

Incorporation of doping ions Ce^{3+} in the host $\text{Sr}_2\text{P}_2\text{O}_7$ can be identified by knowing the alike ionic size of the host ions and the doping ions. In $\text{Sr}_2\text{P}_2\text{O}_7$ phosphor, the ionic radius of Sr^{2+} and P^{5+} ions are to be around 1.31 \AA and 0.52 \AA , whereas the ionic radius of Ce^{3+} ion is 1.19 \AA . In the prepared phosphor, due to the mismatching of the ionic size of Ce^{3+} ion in comparison with P^{5+} ion, the substitution of Ce^{3+} ion in place of P^{5+} ion could result into the deformation of host lattice and the crystal structure [71]. As well as the large difference in ionic charge between the Ce^{3+} ion and P^{5+} ion cannot allow the substitution of Ce^{3+} ion at P^{5+} ion. The ionic size of Ce^{3+} ion in comparison with Sr^{2+} ion marginally smaller, due to the small difference of ionic sizes and ionic charge of Ce^{3+} and Sr^{2+} ions, the substitution of Ce^{3+} ion can take place at Sr^{2+} position without the

altering the structure of host lattice [72, 73]. Substitution of Ce^{3+} ion at two Sr^{2+} sites in the host can be very important to complete the charge compensation between the Ce^{3+} and Sr^{2+} ions.



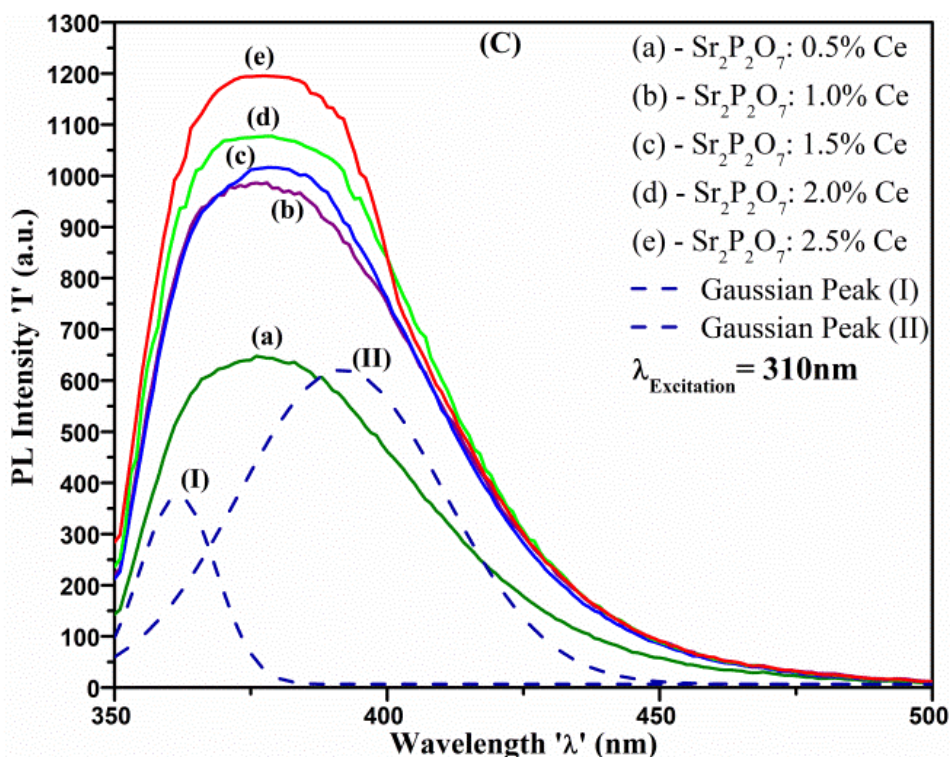


Figure 4.7 PL emission spectra: (A) $\lambda_{\text{Excitation}} = 254$ nm; (B) $\lambda_{\text{Excitation}} = 268$ nm; (C) $\lambda_{\text{Excitation}} = 310$ nm of $\text{Sr}_2\text{P}_2\text{O}_7$: x Ce^{3+} ($x = 0.5, 1.0, 1.5, 2.0$ and 2.5 mol%) phosphor.

As shown in Figure 4.7 (A), (B) and (C), the emission spectra made up of a single broad band which is resolved into two Gaussian peaks centered at 363 and 395 nm perceived upon excitation at 254, 268 and 310 nm. The excitation and emission spectra of Ce^{3+} doped $\text{Sr}_2\text{P}_2\text{O}_7$ phosphor evidently validate that doped Ce^{3+} ions can inhabit two different lattice sites in the host. As the incorporation of Ce^{3+} ions takes place at Sr^{2+} ions sites in the host, i.e., divalent host ion substituted by trivalent impurity ion, necessitates the charge compensatory vacancy because of charge imbalance occurs in the host. In charge compensation procedure two Ce^{3+} ions can be substitute three Sr^{2+} ions, where two Ce^{3+} ions occupy at two strontium sites and leaving a one-site empty [73, 74]. These could be results in the formation of one vacancy in the lattices and incorporation of Ce^{3+} ions results in two types of sites for Ce^{3+} ions in host $\text{Sr}_2\text{P}_2\text{O}_7$ [73, 75]. The emission spectra Ce^{3+} doped $\text{Sr}_2\text{P}_2\text{O}_7$ resolved in two peaks, the emission occurs at a shorter wavelength 363 nm can be attributed to Ce^{3+} ions located at Sr^{2+} site without participation of associated charge compensatory vacancy, while the emission occurs at a longer wavelength 395 nm can be attributed to Ce^{3+} ions occupying Sr^{2+} sites with associated charge compensatory vacancy [76, 77]. The two different Sr^{2+} sites corresponding to with and without charge compensatory vacancy are designated as sites I and II, respectively.

The crystalline environment surrounding doped ions is one of the most important factors for the tuning of the luminescence properties of the phosphors so that the phosphor $\text{Sr}_2\text{P}_2\text{O}_7$ has been doped for the various concentrations of Ce^{3+} [78]. The high similarity in the PL emission spectra of Ce-doped $\text{Sr}_2\text{P}_2\text{O}_7$ for the different concentration of doping ion and various excitation wavelengths verifies the structural and compositional similarity of the phosphors which is also illustrated by structural characterization.

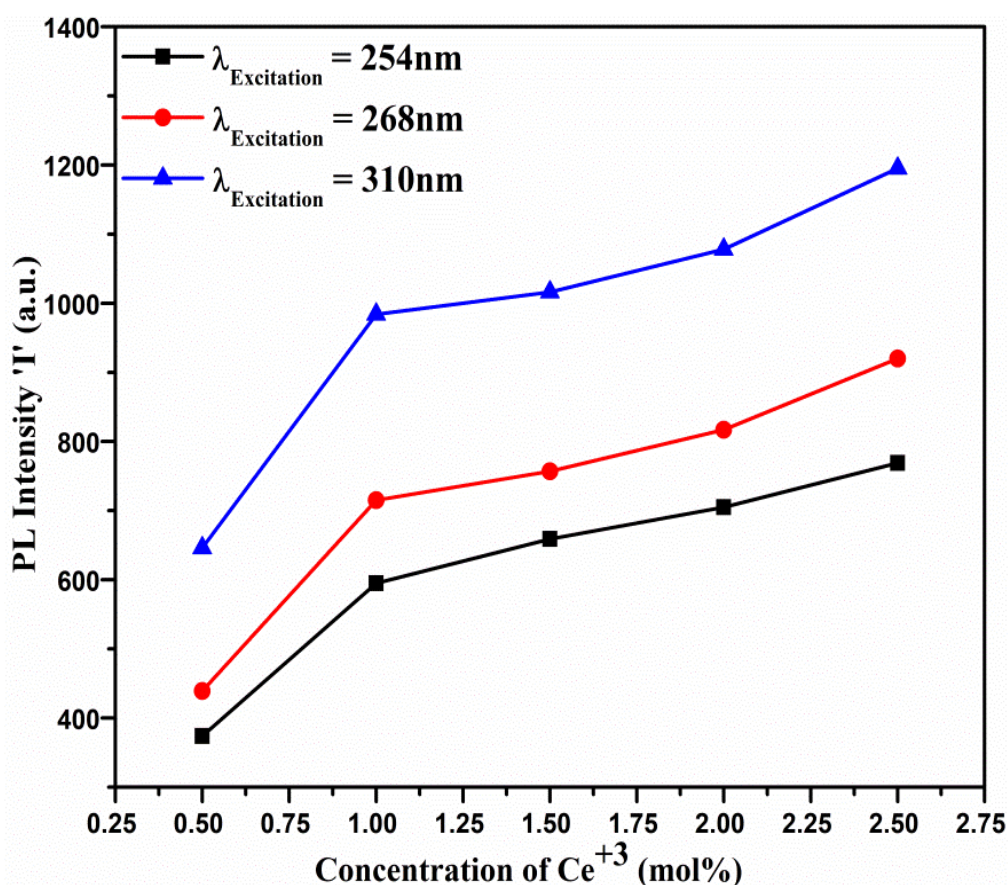


Figure 4.8 Plot of PL emission intensity (I) vs Concentration of Ce^{3+} in $\text{Sr}_2\text{P}_2\text{O}_7$ phosphor.

The PL emission intensity varies accordingly with respect to the excitation energy and the concentration of Ce^{3+} ion. Broadening in PL emission band is observed due to the lowest crystal field component of the $5d^1$ configuration to the two distinct levels of ground state. Stokes shift mainly occurs due to the ideal spectroscopic characteristics of Ce^{3+} and incorporate Ce^{3+} into the host material. RE-activated phosphor materials are subject to renewed research interest and cerium makes a large contribution to this interest in UV emission phosphors [79]. The graph of PL emission intensity vs doping ion concentration for various excitation energy is shown in Figure 4.8. The maximum

intensity of the PL emission band of α - $\text{Sr}_2\text{P}_2\text{O}_7$ increases linearly with the increase in the concentration of Ce^{3+} ion when the doping level varies between 1.0 and 2.5 mol%. These could occur due to highly populated 5d–4f allowed electronic transitions which can be increased with the escalation in the doping concentrations of Ce^{3+} . A graph shown in Figure 4.8 indicates that PL intensity also decreases with the excitation energy, i.e. towards shorter wavelengths site. This could be resulting due to the density of the optical electronic transition decreases with higher excitation energies or due to the increases in the nonradiative transitions at higher excitation energy. Figure 4.9 shows the graph of PL intensity vs crystallite size of Ce^{3+} in $\text{Sr}_2\text{P}_2\text{O}_7$. It shows that the PL intensity is high for the higher concentration where the crystallite size is lesser. In another word, the PL intensity increases as the crystallite size decrease. Thus the PL intensity of Ce^{3+} in $\text{Sr}_2\text{P}_2\text{O}_7$ significantly depends on the crystallite size.

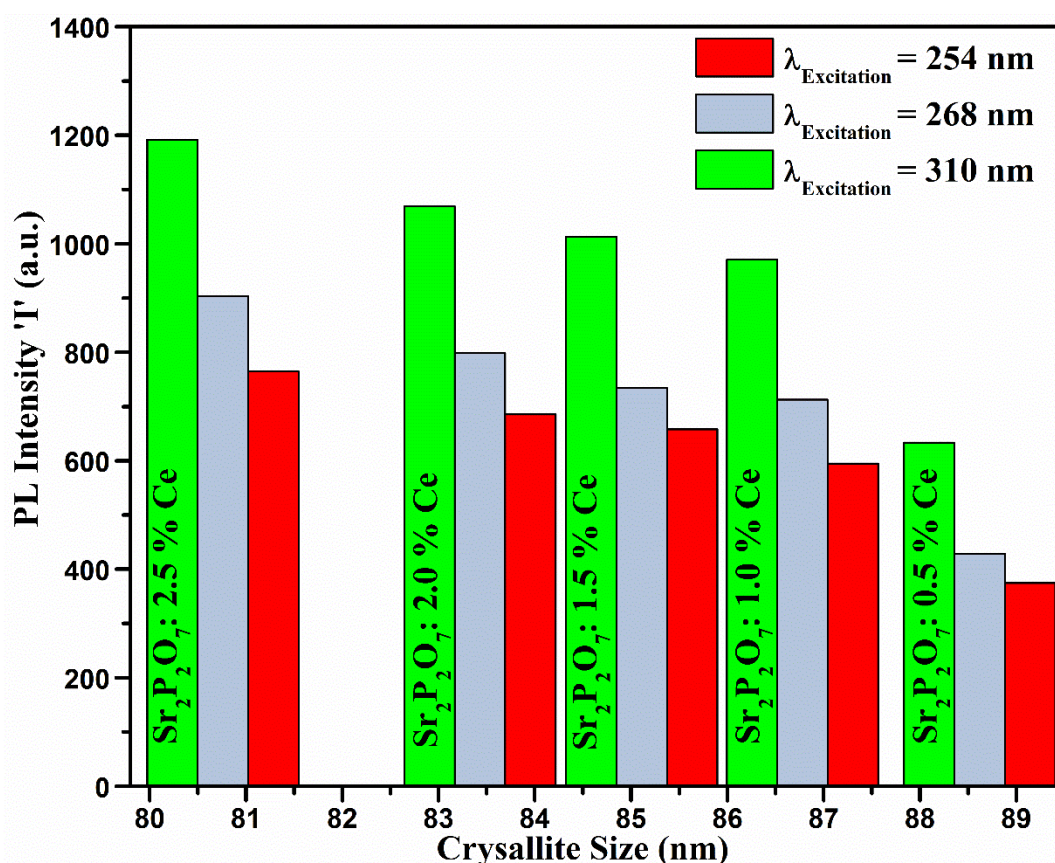


Figure 4.9 Plot of PL emission intensity (I) vs Crystallite Size of Ce^{3+} in $\text{Sr}_2\text{P}_2\text{O}_7$ phosphor.

The calculated CIE coordinates of Ce^{3+} -doped $\text{Sr}_2\text{P}_2\text{O}_7$ phosphor in violet region for all excitation wavelength 254, 268 and 310 nm. CIE coordinates are (X = 0.283, Y =

0.161), ($X = 0.275$, $Y = 0.165$) and ($X = 0.272$, $Y = 0.170$) for 254, 268 and 310 nm excitation wavelength respectively. This indicates that Ce^{3+} doped $\text{Sr}_2\text{P}_2\text{O}_7$ phosphor exhibits violet emission under UV excitation which gives its potential application for UV LED phosphor.

4.3.2. $\text{Sr}_2\text{P}_2\text{O}_7: \text{Eu}^{3+}$

Figure 4.10 shows the excitation spectra of $\text{Sr}_2\text{P}_2\text{O}_7: x \text{Eu}^{3+}$ ($x = 0.5, 1.0, 1.5, 2.0, 2.5$ and 5.0 mol%) recorded at 618 nm emission wavelength at room temperature. The excitation spectra consist of a broad band and some sharp lines in the UV-Blue range 350-500 nm. The excitation spectra of the phosphor show predominant excitation under the ${}^5\text{D}_0$ - ${}^7\text{F}_2$ (618 nm) emission of Eu^{3+} ions and it can remain constant for all doping concentration. The excitation intensity is been prominent for the high concentration of 5.0 mol% Eu^{3+} , it reveals absorption of incident photons increases with the increase in doping concentration. The broad band centered at 266 nm could be attributed due to the charge-transfer transition band of doping ion and oxygen ion of the host lattice (Eu^{3+} - O^2) [80]. The energy of the charge transfer state (CTS) essentially depends on the environments of host surrounding the doping ion. The energies of CTS and 4f states of trivalent rare earth ion are the relatively same for rare-earth ions in any host materials.

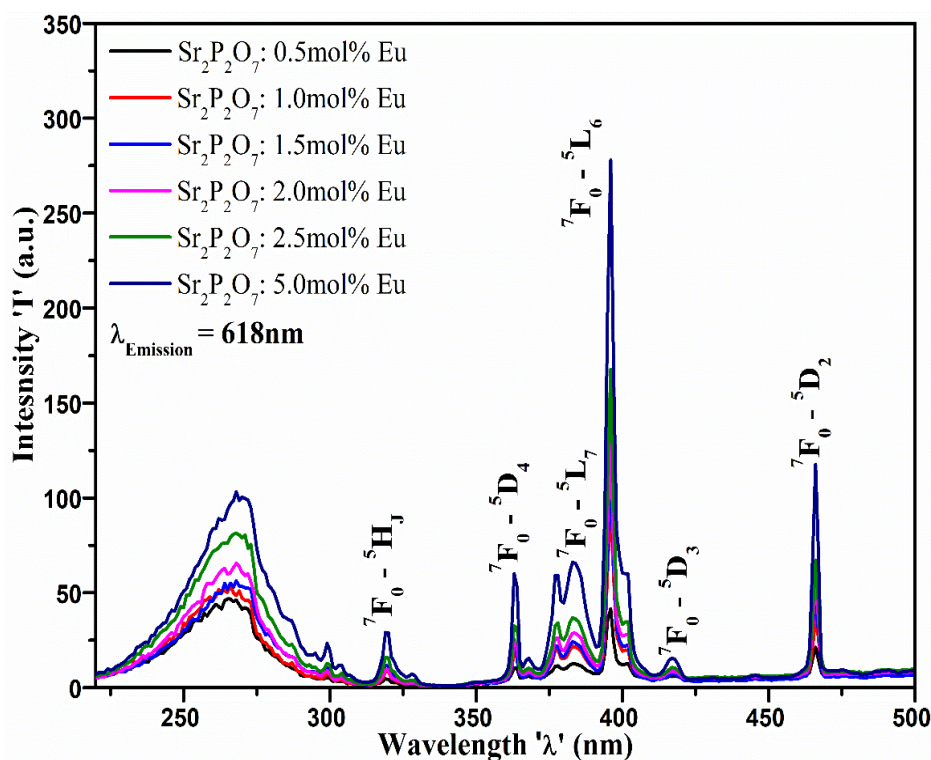
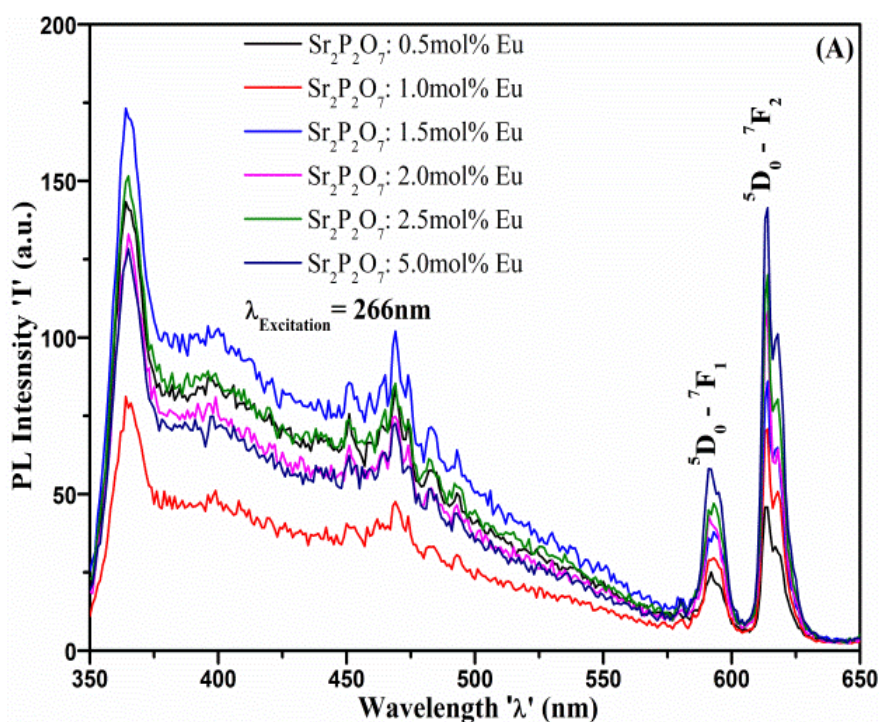


Figure 4.10 Excitation spectra of $\text{Sr}_2\text{P}_2\text{O}_7: x \text{Eu}^{3+}$ ($x = 0.5, 1.0, 1.5, 2.0, 2.5$ and 5.0 mol%) phosphor.

As shown in Figure 4.10, the broad band excitation with maximum peak intensity at 266 nm is occurred due to CTS, where the charge transfer from host Sr^{2+} to dopant Eu^{3+} . The energy of excitation peak is $37.6 \times 10^3 \text{ cm}^{-1}$ and it is comparable to that of the energy of commercial phosphor $40 \times 10^3 \text{ cm}^{-1}$. As a result, CTS interact with 4f states and it can lead to f-f emissions [22]. The excitation spectra contain discrete sharp lines due to the characteristic 4f–4f transitions of Eu^{3+} ion at 396 nm (${}^7\text{F}_0$ – ${}^5\text{L}_6$) and 466 nm (${}^7\text{F}_0$ – ${}^5\text{D}_2$) indicating that $\text{Sr}_2\text{P}_2\text{O}_7:\text{Eu}^{3+}$ can be efficiently excited by UV-blue LED (350–480 nm) and blue-LED chips (465 nm). The excitation spectra also contain several small excitation lines ascribed due to the ${}^7\text{F}_0$ – ${}^5\text{D}_4$ (363 nm), ${}^7\text{F}_0$ – ${}^5\text{L}_7$ (383 nm), and ${}^7\text{F}_0$ – ${}^5\text{D}_3$ (417 nm) transitions of Eu^{3+} ions. The phosphors for LED application should be excited in the range of the near violet-blue region of the excitation spectra [81, 82]. The prominent red-emitting UV-LED phosphor exhibit absorption at 395 nm (i.e., LED excitation wavelength) are potential for orange-red LED.

The PL emission spectra of $\text{Sr}_2\text{P}_2\text{O}_7: x\% \text{Eu}^{3+}$ measured upon the excitation wavelength 266 nm, 396 nm and 466 nm are shown in Figure. 4.11 (A), (B), (C) respectively. The PL emission spectra for excitation wavelength 266 nm (Figure. 4.11 (A)) contain strong PL emission peak observed for different excitations is located at 618 nm, attributed to the ${}^5\text{D}_0$ – ${}^7\text{F}_2$ characteristic transition of Eu^{3+} ion and the weak PL emission peak at 595 nm is attributed to the ${}^5\text{D}_0$ – ${}^7\text{F}_1$ transitions of Eu^{3+} due to the $4f^6$ configuration [82, 83].



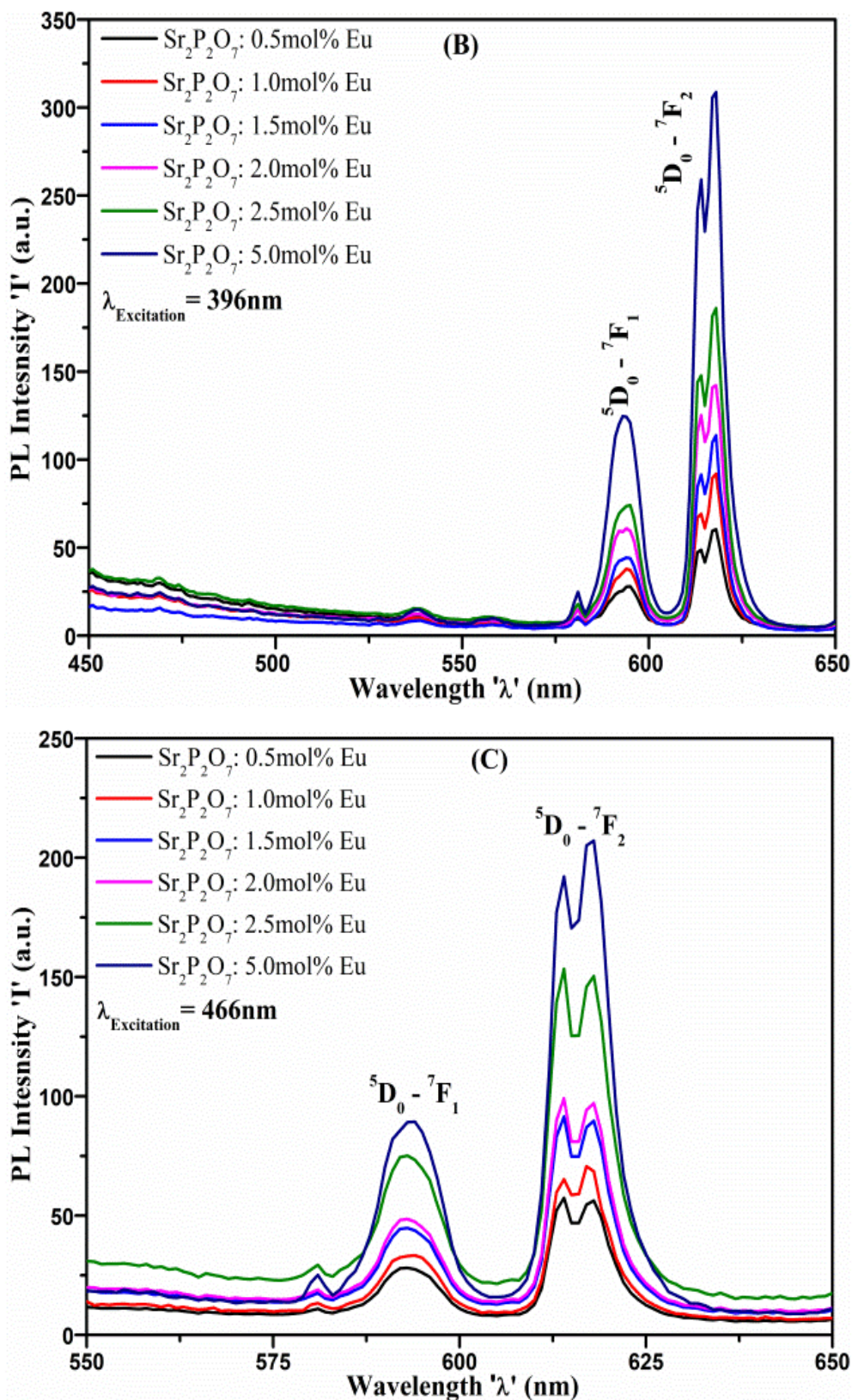


Figure 4.11 PL emission spectra: (A) $\lambda_{\text{Excitation}} = 266\text{ nm}$; (B) $\lambda_{\text{Excitation}} = 396\text{ nm}$; (C) $\lambda_{\text{Excitation}} = 466\text{ nm}$, of $\text{Sr}_2\text{P}_2\text{O}_7 : x\text{Eu}^{3+}$ ($x = 0.5, 1.0, 1.5, 2.0, 2.5$ and 5.0 mol\%) phosphor.

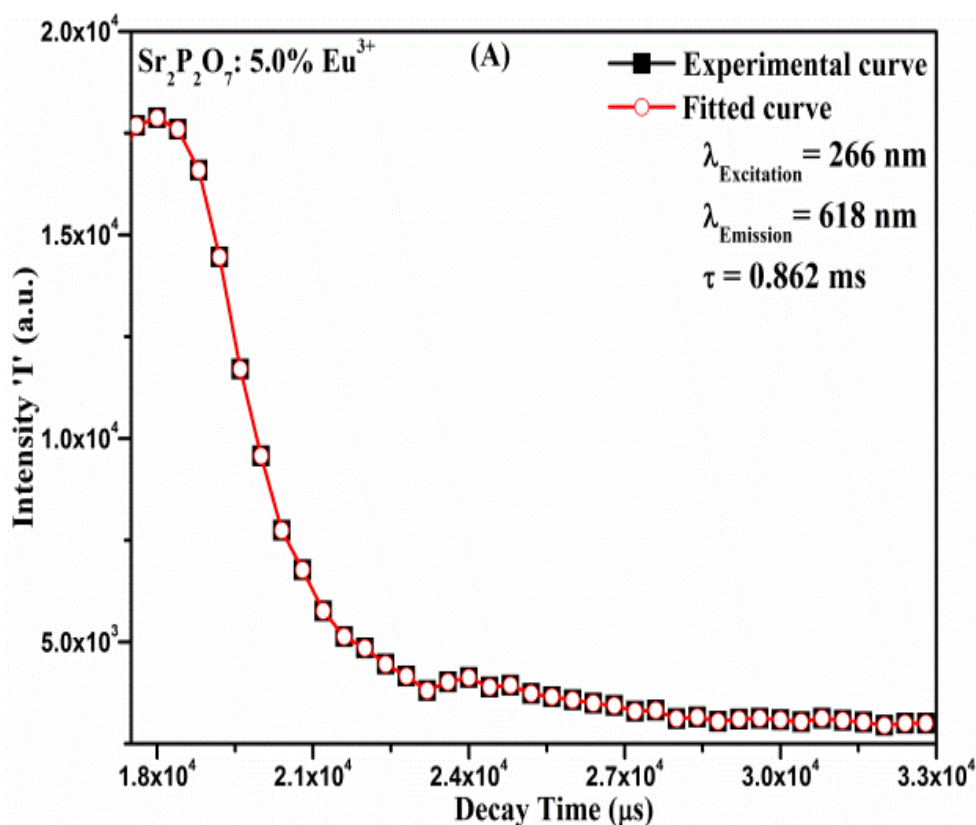
The PL emission spectra of $\text{Sr}_2\text{P}_2\text{O}_7$: x% Eu^{3+} for excitation wavelength 466 nm and 266 nm are not as much intense than that of 396 nm (Figure. 4.11 (B), (C)), as well as the PL emission intensity of characteristic transitions of Eu^{3+} is mainly depends upon the doping concentration of Eu^{3+} in host $\text{Sr}_2\text{P}_2\text{O}_7$. The behavior of Eu^{3+} ion in the phosphor is hypersensitive to the local chemical environment according to the Judd–Ofelt theory [84-86]. The site symmetry of Eu^{3+} ion inside the microstructures of host lattice has an influence on the luminescence efficiency of Eu^{3+} -activated hosts. The magnetic dipole transition ($^5\text{D}_0$ - $^7\text{F}_1$) is significant when Eu^{3+} ion occupies an inversion symmetry site in host $\text{Sr}_2\text{P}_2\text{O}_7$ i.e., centrosymmetric in the host lattice. The electric-dipole transition ($^5\text{D}_0$ - $^7\text{F}_2$) is significant when Eu^{3+} ion in the host is subjected without an inversion center i.e., non-centrosymmetric in host lattice [87-90]. The prediction of site symmetry of Eu^{3+} ion in the host lattice can be identified by the integral intensity ratio $R = I(^5\text{D}_0$ - $^7\text{F}_2) / I(^5\text{D}_0$ - $^7\text{F}_1)$, where $I(^5\text{D}_0$ - $^7\text{F}_2)$ is the intensity of electric dipole transition and $I(^5\text{D}_0$ - $^7\text{F}_1)$ is the intensity of magnetic dipole transition [91, 92]. As the magnitude of the integral ratio is high enough, then occupancy of Eu^{3+} in the non-centrosymmetric site is much higher than that of the centrosymmetric site in the host lattice. The PL emission peak intensity of the $^5\text{D}_0$ - $^7\text{F}_2$ (618 nm) transition is much stronger than that of the peak intensity of the $^5\text{D}_0$ - $^7\text{F}_1$ (595 nm) transition. The integral intensity ratio ‘R’ of Eu^{3+} doped $\text{Sr}_2\text{P}_2\text{O}_7$ phosphors for different excitation wavelength is been ranging from 2 to 2.6. It reveals that the Eu^{3+} ions could be occupied at the non-centrosymmetric sites within the crystal structure of $\text{Sr}_2\text{P}_2\text{O}_7$ [93-97]. The experimental results of PL emission revealed that the percentage of the non-centrosymmetric site is much higher than that of the centrosymmetric site for the higher concentration of doping. Doped Eu^{3+} ions in phosphors can occupy the sites that have noninversion symmetry and the intense red emission due to the electric dipole transition is utilized for practical applications [22]. The maximum sensitivity of the human eye to sense spectral luminous wavelength is about 555 nm. As the spectral luminous move towards the longer wavelengths i.e, in the red region, the sensitivity falls quickly. The red emission made up of narrow sharp spectral lines could be the brighter appearance to the human eye than that of the broad red emission having the identical red color chromaticity and emission energy. To achieve the ideal red emission of color TV to be used in the NTSC system, the red chromaticity standard has been fixed at the coordinates $x = 0.67$, $y = 0.33$ which can obtain by the

ideal emission spectra of a narrow band around 610 - 630 nm in Eu^{3+} doped phosphors [23].

The emission spectrum of the $\text{Sr}_2\text{P}_2\text{O}_7: x\% \text{Eu}^{3+}$ shown in Figure. 4.11 (A), (B) and (C) excited under the excitation wavelength 266, 396 and 466 nm respectively, exhibit a strong red emission band at 618 nm assigned to the $^5\text{D}_0\text{-}^7\text{F}_2$ transition and weak band at 595 nm consequent to the $^5\text{D}_0\text{-}^7\text{F}_1$ transition. The fitted PL decay curves for the red emission sharp band $^5\text{D}_0\text{-}^7\text{F}_2$ (618 nm) under the different excitation wavelength of 5.0mol% Eu^{3+} doped $\text{Sr}_2\text{P}_2\text{O}_7$ is shown in Figure. 4.12. The PL emission decay curve of the phosphor gives information about the relaxation dynamics of the phosphor in the excited state. Relaxation process of excited states of doped trivalent rare earth ions in phosphor materials is taking place by radiative decay, multiphonon relaxation and non-radiative ion-ion interaction [98]. The experimental decay curve is been fitted by a single-exponential function using the following equation,

$$I = I_0 e^{-\frac{t}{\tau}}$$

Where I is the PL emission intensity, I_0 is a PL emission intensity at time $t = 0$ s, t is the time and τ is the decay time for the exponential component [3, 88].



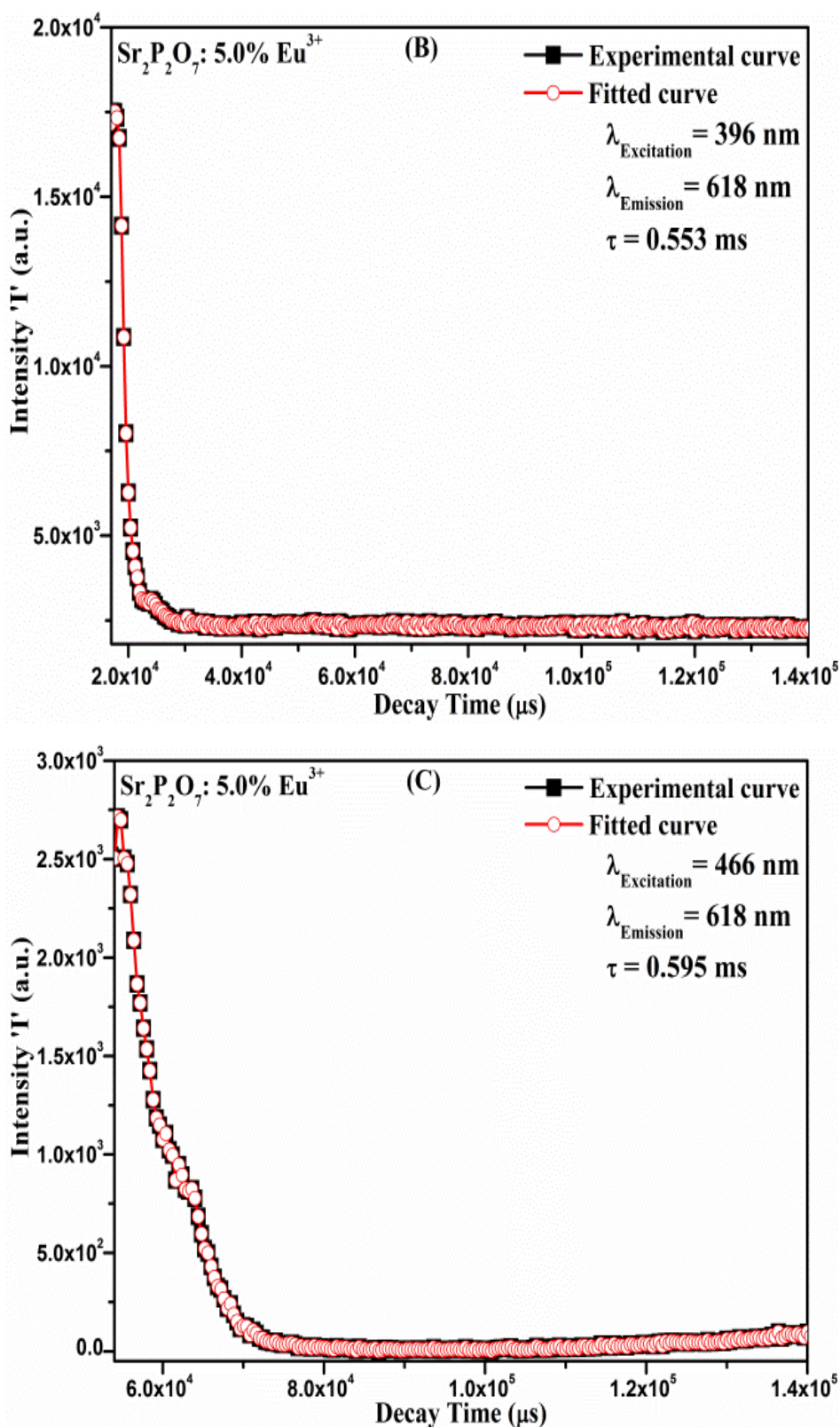


Figure 4.12 The decay curves of Sr₂P₂O₇: 5.0% Eu³⁺ phosphor: (A) Excited at 266 nm, Monitored at 618 nm; (B) Excited at 396 nm, Monitored at 617 nm; (C) Excited at 466nm, Monitored at 618 nm.

The measured values of the decay time are 0.862 ms for 266 nm excitation, 0.553 ms for 396 nm excitation, 0.595 ms for 466 nm excitation. In Eu^{3+} doped $\text{Sr}_2\text{P}_2\text{O}_7$ phosphor, due to a combination of spin states and parity states of the doping ion Eu^{3+} occupying a non-centrosymmetric site inside the host lattice, as a result, the parity forbidden transition ${}^5\text{D}^0 - {}^7\text{F}^2$ becomes partly allowed and leading to the faster decay time to the ground state [99].

The CIE (Commission International de l'Eclairage) chromaticity coordinate diagram of $\text{Sr}_2\text{P}_2\text{O}_7: 5.0\% \text{Eu}^{3+}$ is shown in Figure. 4.13. The CIE coordinates and site symmetry ratio of $\text{Sr}_2\text{P}_2\text{O}_7: x\% \text{Eu}^{3+}$ phosphors are mention in Table 4.2 for different concentration of doping ions and excitation wavelength. The CIE color coordinate value of $\text{Sr}_2\text{P}_2\text{O}_7: x\% \text{Eu}^{3+}$ under 466 nm excitation wavelength is very similar to that of the NTSC system which is lying in the red region of the color chromaticity. The CIE coordinate value of $\text{Sr}_2\text{P}_2\text{O}_7: x\% \text{Eu}^{3+}$ under 396 nm excitation wavelength is exhibited in the orange-red region of the color chromaticity and under 266 nm excitation wavelength exhibits in the yellow region of the color chromaticity.

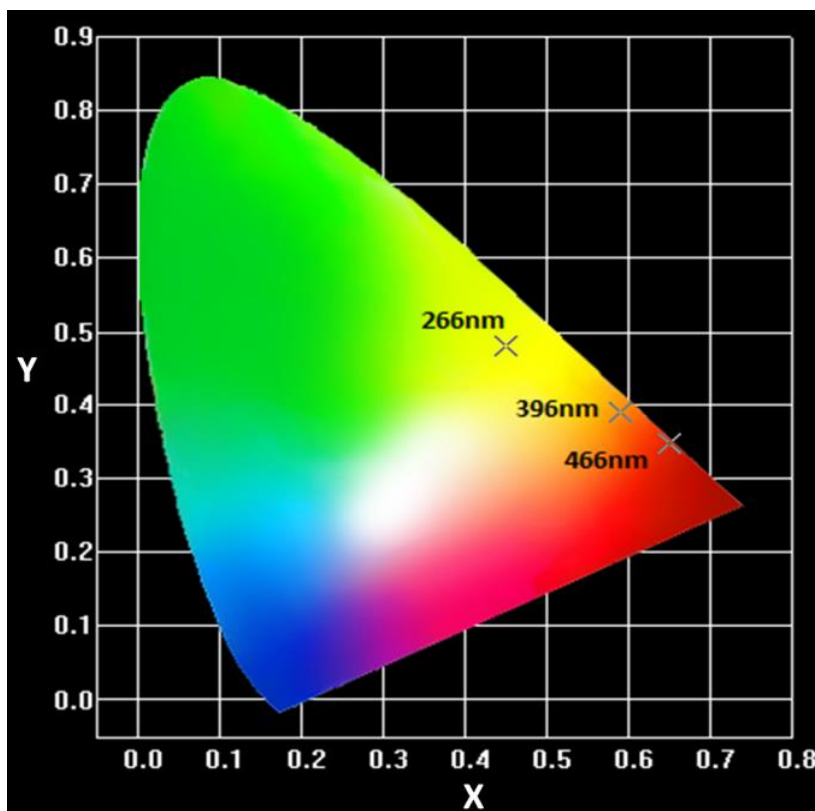


Figure 4.13 CIE chromaticity coordinate diagram of $\text{Sr}_2\text{P}_2\text{O}_7: 5.0\% \text{Eu}^{3+}$ phosphor.

Sample	Excitation Wavelength	CIE co-ordinates		CCT (K)	R
		X	Y		
Sr ₂ P ₂ O ₇ :0.5% Eu ³⁺	266 nm	0.443	0.469	3355	2.08
	396 nm	0.593	0.372	1772	2.16
	466 nm	0.666	0.339	3146	2.05
Sr ₂ P ₂ O ₇ :1.0% Eu ³⁺	266 nm	0.448	0.467	3269	2.44
	396 nm	0.595	0.381	1741	2.56
	466 nm	0.662	0.338	3115	2.12
Sr ₂ P ₂ O ₇ :1.5% Eu ³⁺	266 nm	0.445	0.462	3283	2.49
	396 nm	0.591	0.387	1721	2.58
	466 nm	0.661	0.337	3135	2.17
Sr ₂ P ₂ O ₇ :2.0% Eu ³⁺	266 nm	0.451	0.473	3261	2.51
	396 nm	0.592	0.385	1725	2.60
	466 nm	0.663	0.332	3370	2.22
Sr ₂ P ₂ O ₇ :2.5% Eu ³⁺	266 nm	0.445	0.471	3337	2.55
	396 nm	0.593	0.390	1718	2.61
	466 nm	0.659	0.338	3065	2.25
Sr ₂ P ₂ O ₇ :5.0% Eu ³⁺	266 nm	0.451	0.479	3296	2.57
	396 nm	0.591	0.391	1715	2.67
	466 nm	0.667	0.335	3319	2.31

Table 4.2 CIE chromaticity coordinates and the integral intensity ratio of transition ⁵D₀-⁷F₂ to ⁵D₀-⁷F₁ of Sr₂P₂O₇:xEu³⁺ phosphor for different excitation wavelength.

As the amount of doping concentration of Eu³⁺ ion increases, the PL emission intensity of ⁵D₀-⁷F₂ transition of Eu³⁺ doped Sr₂P₂O₇ monitored under three different excitation wavelength is increased as shown in Figure. 4.14. There no concentration quenching effect is observed up to the maximum concentration of 5.0% of Eu³⁺ ion. The reason for the increase in intensity can resulting due to the percentage increase of radiative transitions of ⁵D₀-⁷F₂. Figure 4.15 shows the graph of PL emission intensity (I) vs Crystallite Size of Eu³⁺ in Sr₂P₂O₇ phosphor. It indicates that the PL intensity increases as the crystallite size of the phosphor decrease at high doping concentration.

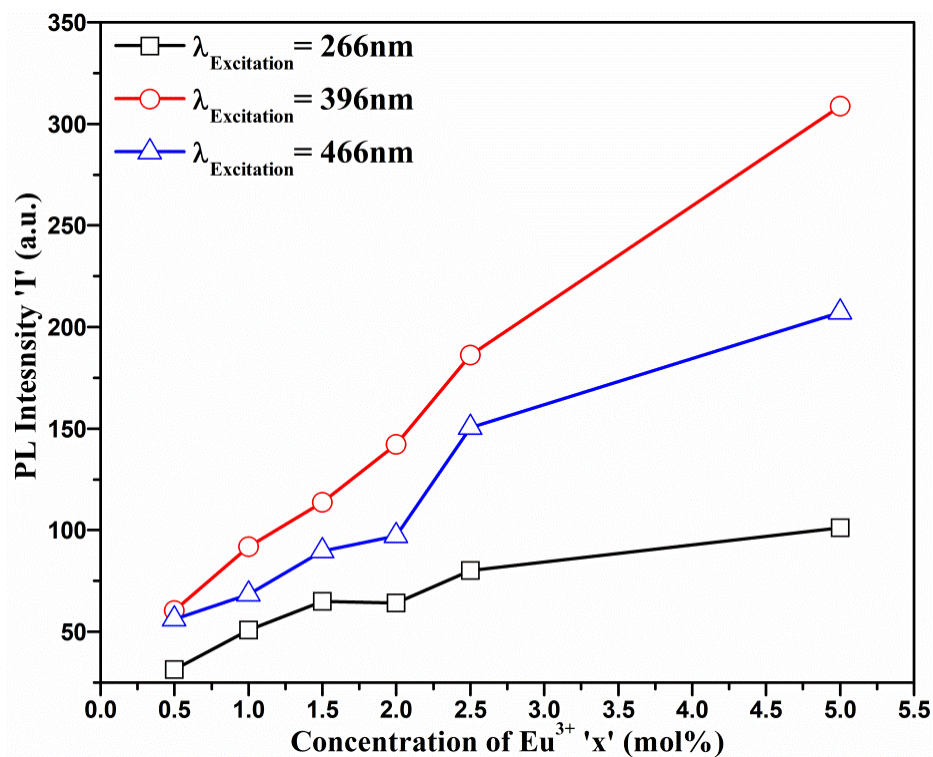


Figure 4.14 PL emission intensity (I) → Concentration of Eu³⁺ graph of Eu³⁺ doped Sr₂P₂O₇ phosphor.

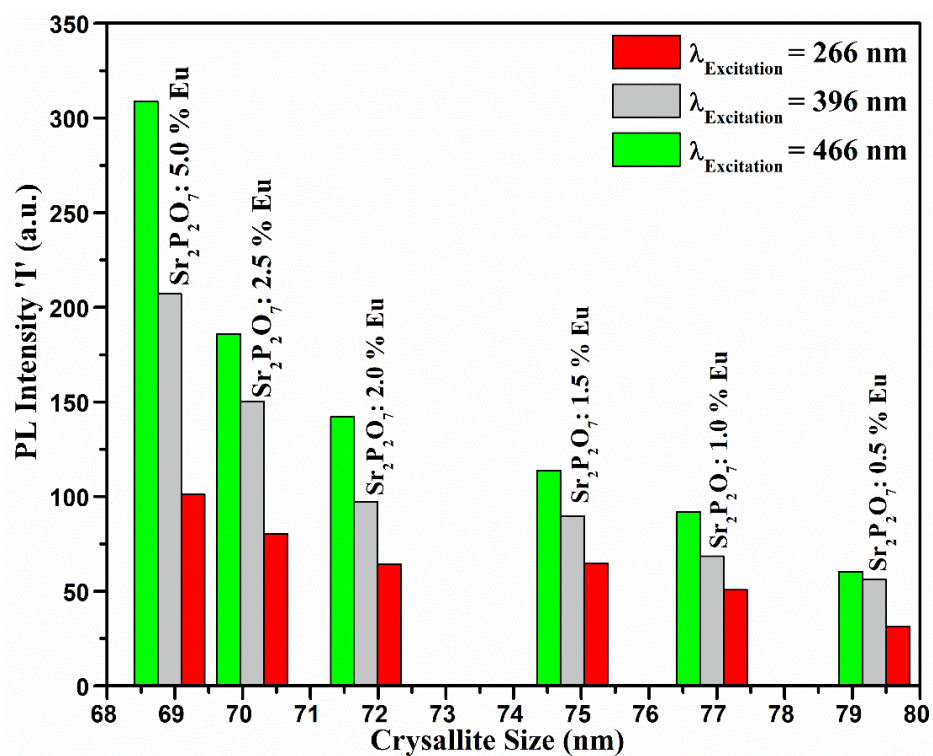


Figure 4.15 Plot of PL emission intensity (I) → Crystallite Size of Eu³⁺ in Sr₂P₂O₇ phosphor.

4.3.3. Tb^{3+} -doped $Sr_2P_2O_7$

Figure 4.16 shows the excitation spectrum of Tb^{3+} -doped $Sr_2P_2O_7$, recorded by monitoring the phosphor by green emission at 547 nm. The excitation spectra display only single band centered at 232 nm which could be ascribed to the ${}^7F_6 \rightarrow {}^9E$ electronic transitions, that can be attributed to the $4f^8 \rightarrow 4f^7 - 5d^1$ spin allowed the transition of Tb^{3+} . Whereas the 9E states can come from the splitting of $4f^7 5d$ state in the crystal field with D_2 symmetry inside the host. An excitation band illustrates that the phosphor can be excited through the UV light of about 232 nm. Generally the intensity f–d transitions is much intense compared to that of the f–f transitions for low concentration of doping of Tb^{3+} ion. Although the intensity of f–d transitions is much weaker compared to that of the f–f transitions for a high concentration of doping of Tb^{3+} concentration. This could come about because of the f–f transitions are forbidden transition while the f–d transitions are allowed according to the Laporte's rule [100]. PL emission spectra of all Tb^{3+} doped $Sr_2P_2O_7$ samples were monitored by exciting peak maximum wavelength i.e., 232 nm to determine the optimum PL emission of the doped phosphors as well as the preparation process based for different concentration of doping ion.

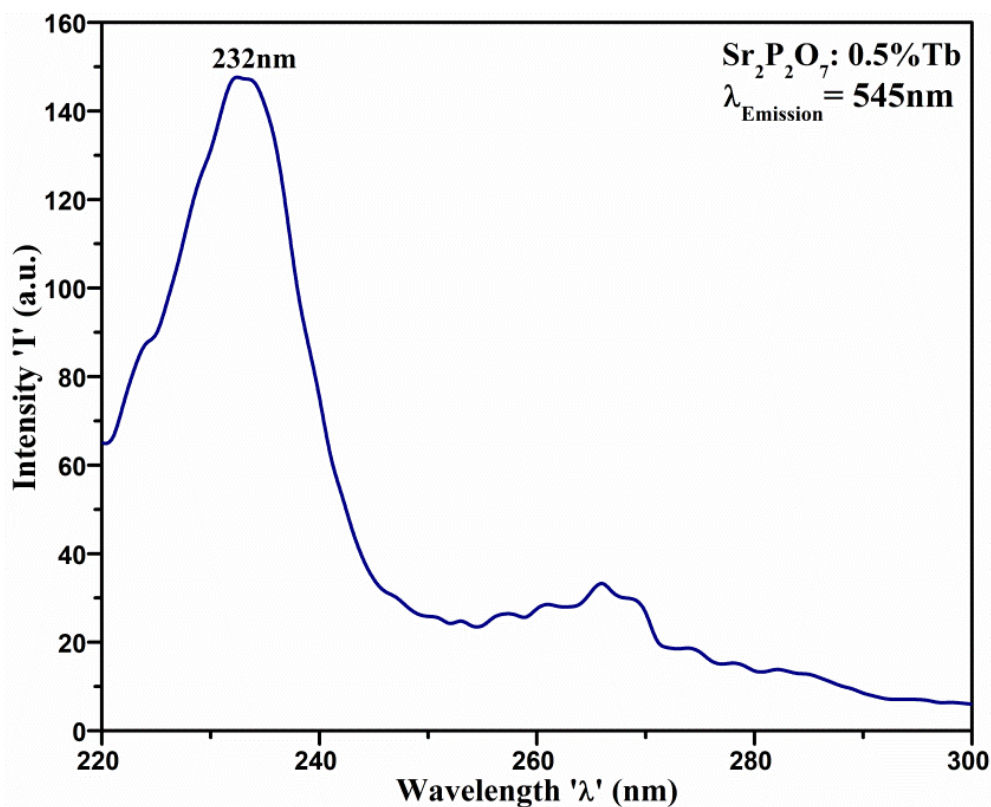


Figure 4.16 PL excitation spectra of $Sr_2P_2O_7$: 0.5 % Tb^{3+} phosphor for $\lambda_{\text{Emission}} = 545$ nm.

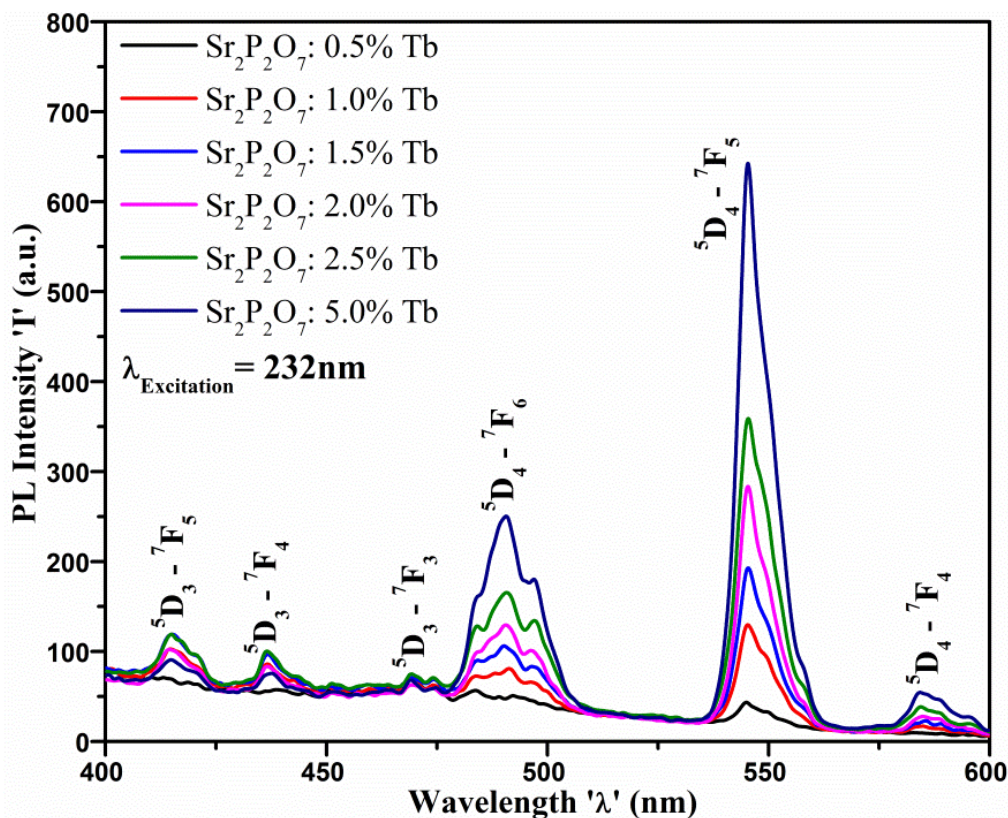


Figure 4.17 PL emission spectra of $\text{Sr}_2\text{P}_2\text{O}_7: x\% \text{Tb}^{3+}$ ($x = 0.5, 1.0, 1.5, 2.0, 2.5, 5.0$) phosphor for $\lambda_{\text{Excitation}} = 232 \text{ nm}$.

Figure 4.17 shows PL emission spectra $\text{Sr}_2\text{P}_2\text{O}_7: x\% \text{Tb}^{3+}$ ($x = 0.5, 1.0, 1.5, 2.0, 2.5, 5.0$) phosphor monitored at $\lambda_{\text{Excitation}} = 232 \text{ nm}$. PL emission spectra demonstrates the several sharp peaks centered at 415, 436, 469, 491, 545 and 584 nm as a consequence of the characteristics radiative transitions of Tb^{3+} ion which can be attributed to the electron transitions taking place correspond to the ${}^5\text{D}_3 \rightarrow {}^7\text{F}_5$, ${}^5\text{D}_3 \rightarrow {}^7\text{F}_4$, ${}^5\text{D}_3 \rightarrow {}^7\text{F}_3$, ${}^5\text{D}_4 \rightarrow {}^7\text{F}_6$, ${}^5\text{D}_4 \rightarrow {}^7\text{F}_5$, and ${}^5\text{D}_4 \rightarrow {}^7\text{F}_4$, respectively. PL emission spectra consist of two groups of emission lines; first group of lines is located in the wavelength range 400 – 475 nm which is consigned to the ${}^5\text{D}_3 \rightarrow {}^7\text{F}_J$ ($J = 5, 4, 3$) electron transitions of Tb^{3+} , second group of lines are located in the wavelength range of 475 – 600 nm which is resulting due to ${}^5\text{D}_4 \rightarrow {}^7\text{F}_J$ ($J = 6, 5, 4$) electron transitions of Tb^{3+} . It is found that the emission takes place due to ${}^5\text{D}_4 \rightarrow {}^7\text{F}_J$ ($J = 6, 5, 4$) transitions are much stronger than that of ${}^5\text{D}_3 \rightarrow {}^7\text{F}_J$ ($J = 5, 4, 3$) transitions. Sharp emission attributed to the predominant ${}^5\text{D}_4 \rightarrow {}^7\text{F}_5$ transition at about 545 nm which can be resulting due to the most probable electron transition take place in Tb^{3+} ion. PL emission spectra Tb^{3+} of $\text{Sr}_2\text{P}_2\text{O}_7$ phosphor illustrate that as the doping concentration Tb^{3+} is increased the PL emission intensity in the range 400 – 475 nm increases poorly

as compared to that of the PL emission intensity in the range 475 – 600 nm. The reduction in PL intensity observed in level 5D_3 as the concentrations of Tb^{3+} ion increases can give the evidence for the presence of energy transfer due to cross-relaxation take place between level 5D_3 and 5D_4 [101, 102]. In the phenomenon of the cross-relaxation energy transfer process, the excited ion transfers its partial energy to another ion [50]. This process generally observed in Tb^{3+} ion doped phosphors where the energy transfer occurs between two Tb^{3+} ions situated at a certain distance, as the $Tb^{3+} - Tb^{3+}$ ion distance increases the cross relaxation mechanism reduces. The distance between to ions mainly depends on the host lattice structure. As explained in x-ray diffraction of rare earth doped $Sr_2P_2O_7$, the reduction is observed in lattice constants and the crystallite size of the phosphor due to the increase in the concentration of doping ion. That implies as the doping concentration increases the accumulation of doping ion in the phosphor increases and the crystallite size decreases which can result in the large density of doping ion. Therefore the possibility of cross-relaxation interaction between two close ions immensely increases. The plot of the relation between crystallite size and PL emission intensity is shown in Figure 4.18 that revealed the PL intensity also increases with decreasing crystallite size for a higher concentration of doping Tb^{3+} ion.

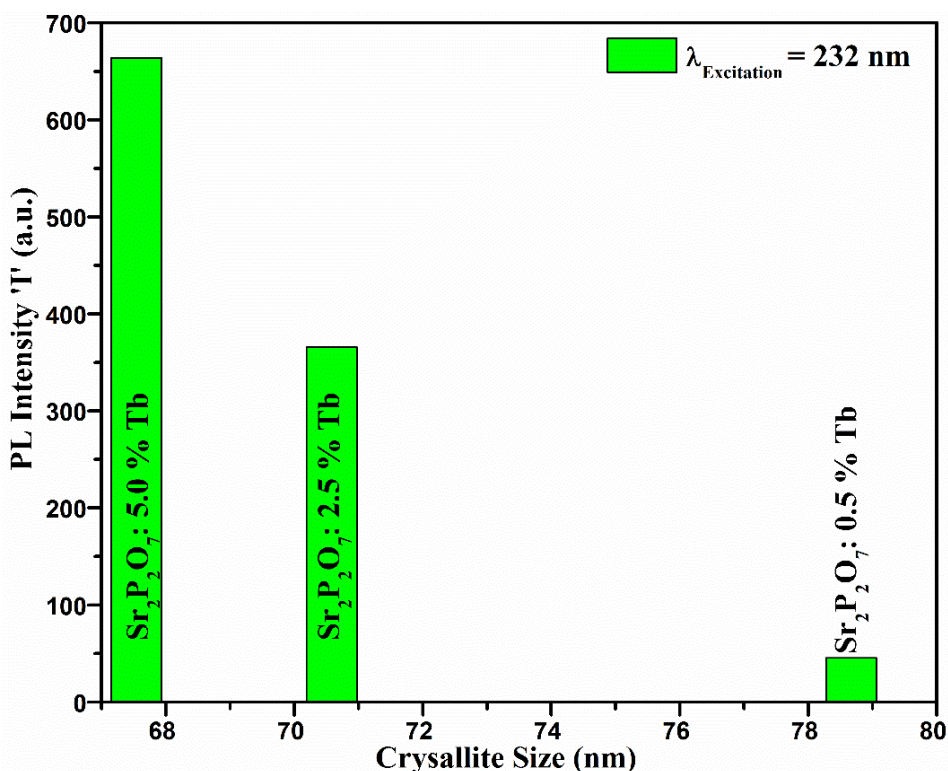


Figure 4.18 Plot of PL emission intensity (I) → Crystallite Size of Tb^{3+} in $Sr_2P_2O_7$ phosphor.

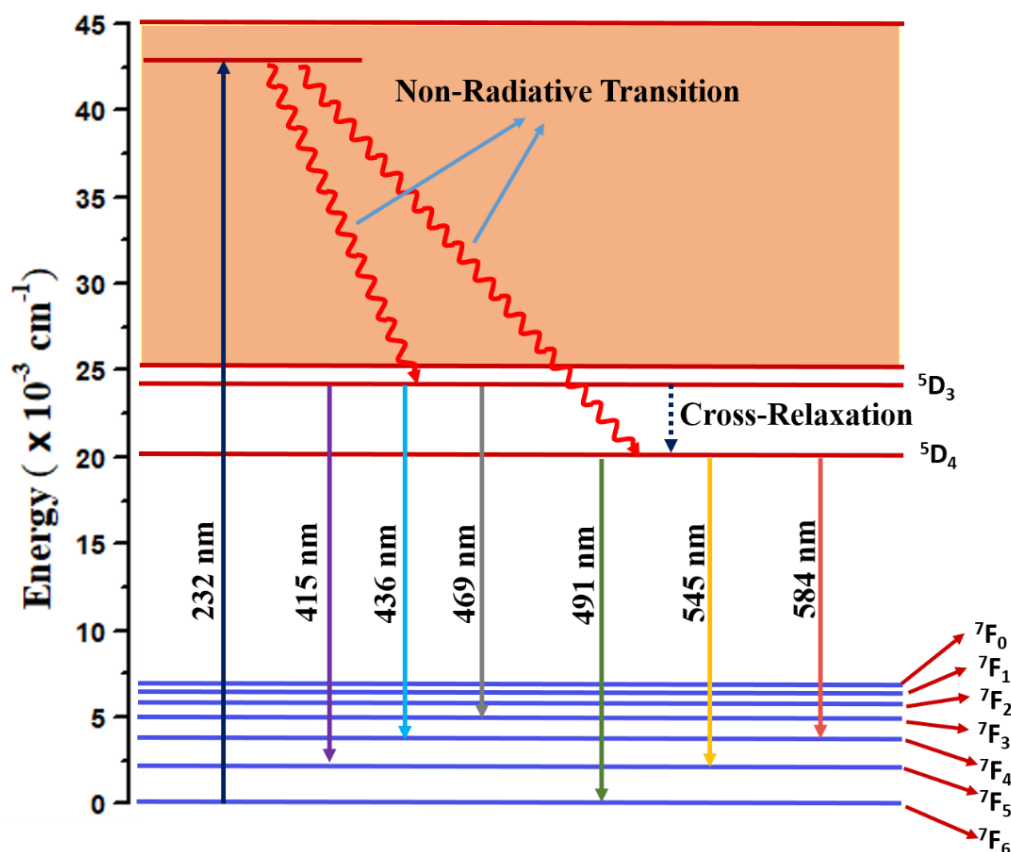


Figure 4.19 Energy level diagram of Sr₂P₂O₇: Tb³⁺ phosphor.

In cross-relaxation process, the energy difference between the two excited states ⁵D₃ and ⁵D₄ is approximately equal that of the energy difference between the ⁷F₆ ground state and higher ⁷F_J states [4, 103, 104]. The occurrence of cross-relaxation would intensify the population of the ⁵D₄ state and as a result, the minimization of PL intensity of ⁵D₃ compare to PL intensity of ⁵D₄. Figure 4.19 shows the energy level diagram of Tb³⁺ formed in the energy gap of the host Sr₂P₂O₇. It shows absorption of UV radiation of wavelength 232 nm seen as an upward arrow, excited Tb³⁺ ions which is decayed to the ⁵D₃ and ⁵D₄ state through the following non-radiative transition. The PL emission has been induced to the electron transition from ⁵D₃ and ⁵D₄ level to the ⁷F_J (J = 3, 4, 5, 6) level seen as a downward arrow with the maximum wavelength of corresponding emission lines. For the low concentration of Tb³⁺ ions, the ⁵D₄ level is populated solely by the non-radiative transition, while as the concentration of Tb³⁺ ions increases the further cross-relaxation takes place from ⁵D₃ level. Due to the cross-relaxation channel, the energy begins transferred from one excited ion Tb³⁺ to other unexcited ion seen as dotted lines. The energy transfer comes about to the cross-relaxation resulting in strong green emission, which can reveal the doping ion Tb³⁺ substitutes the host Sr²⁺ ion site

without any structural deformation. The doping ions occupy the host lattice site and create metastable states inside the energy gap of the host, which is the reason for the occurrence of PL emissions.

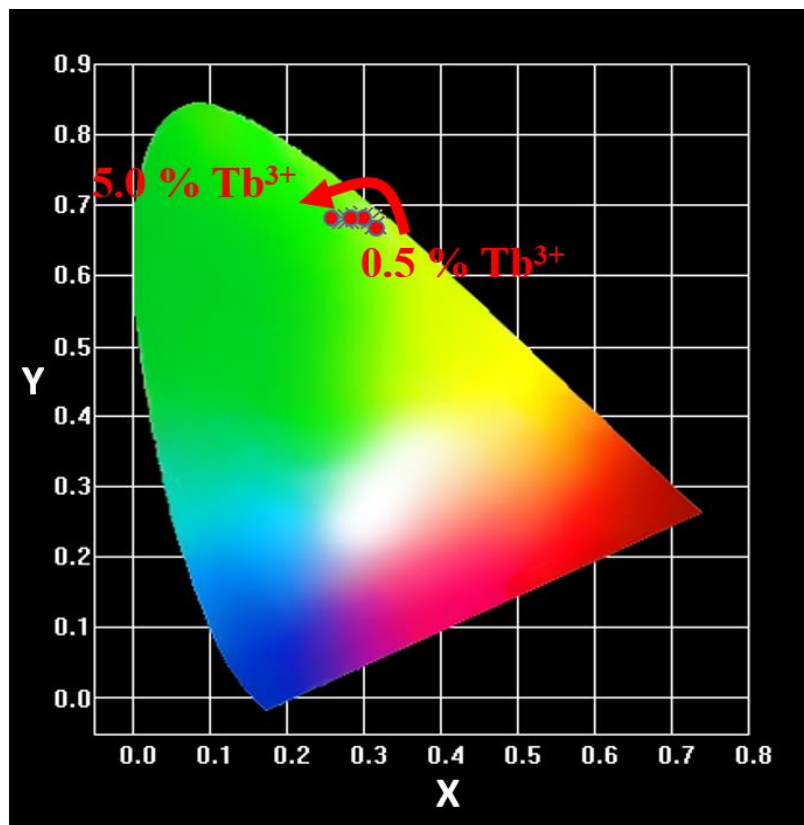


Figure 4.20 CIE chromaticity coordinate diagram of $\text{Sr}_2\text{P}_2\text{O}_7: x\% \text{Tb}^{3+}$ phosphor.

Sample	CIE co-ordinates		Emission Color
	X	Y	
$\text{Sr}_2\text{P}_2\text{O}_7: 0.5\% \text{Tb}^{3+}$	0.316	0.673	Green
$\text{Sr}_2\text{P}_2\text{O}_7: 1.0\% \text{Tb}^{3+}$	0.309	0.681	
$\text{Sr}_2\text{P}_2\text{O}_7: 1.5\% \text{Tb}^{3+}$	0.299	0.685	
$\text{Sr}_2\text{P}_2\text{O}_7: 2.0\% \text{Tb}^{3+}$	0.291	0.682	
$\text{Sr}_2\text{P}_2\text{O}_7: 2.5\% \text{Tb}^{3+}$	0.280	0.681	
$\text{Sr}_2\text{P}_2\text{O}_7: 5.0\% \text{Tb}^{3+}$	0.273	0.680	

Table 4.3 CIE chromaticity coordinates of $\text{Sr}_2\text{P}_2\text{O}_7: x\% \text{Tb}^{3+}$ phosphor.

The PL emission color of Tb^{3+} doped $\text{Sr}_2\text{P}_2\text{O}_7$ phosphor was analyzed and confirmed by CIE chromaticity coordinates. Figure 4.20 shows the CIE chromaticity coordinates of Tb^{3+} doped $\text{Sr}_2\text{P}_2\text{O}_7$ phosphor. The calculated CIE coordinates for

different concentrations of Tb^{3+} are situated in a green region where green color enhancement observed with the increment in Tb^{3+} of concentrations. The color coordinates values of Tb^{3+} doped $\text{Sr}_2\text{P}_2\text{O}_7$ phosphor are summarized in Table 4.3. This indicates that Tb^{3+} -doped $\text{Sr}_2\text{P}_2\text{O}_7$ phosphor displays green color under UV excitation at 232 nm. Figure 4.21 exhibits the change occur in PL intensity of two dominant characteristic transitions ${}^5\text{D}_4 - {}^7\text{F}_6$ and ${}^5\text{D}_4 - {}^7\text{F}_5$ due to change in Tb^{3+} ion concentration. It is observed that PL intensity of the emission due to ${}^5\text{D}_4 - {}^7\text{F}_5$ transition is 2–3 times greater than that of the PL intensity of the emission due to ${}^5\text{D}_4 - {}^7\text{F}_6$ transition. The effect concentration quenching of doping ion occurred but the optimized green emission is observed for 5.0% Tb^{3+} ion concentration.

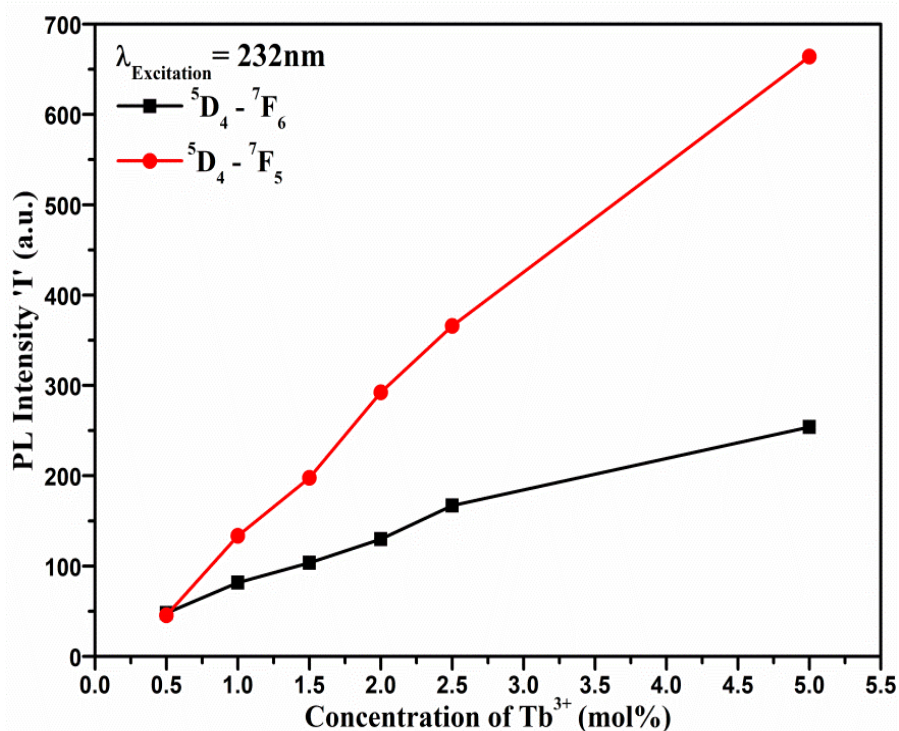


Figure 4.21 PL emission intensity (I) → Concentration of Tb^{3+} in $\text{Sr}_2\text{P}_2\text{O}_7$ phosphor.

Photoluminescence Output of RE^{3+} doped $\text{Sr}_2\text{P}_2\text{O}_7$

The photoluminescence studies for RE^{3+} doped $\text{Sr}_2\text{P}_2\text{O}_7$ phosphors displayed fascinating results, the following are the logical conclusions:

- ❖ Ce^{3+} doped $\text{Sr}_2\text{P}_2\text{O}_7$ phosphor exhibits broad emission around at 385 nm in near UV region under the excitation wavelengths 254, 268 and 310 nm. The broad emission from 360 to 440 nm in UV to the Violet Blue region is observed due to the 5d-4f transitions of Ce^{3+} . The Gaussian fitting of the emission band revealed the energy discrepancy of 2081 cm^{-1} between the two Gaussian peaks located at 363 nm and

395 nm due to the spin-orbital coupling of 4f state. The prominent emission occurs under 310 nm excitation wavelength. The PL emission intensity increases with the doping concentration gives the confirmation of the incorporation of Ce^{3+} increase with higher concentration. The crystallite size affects the PL emission, where the PL emission increases with decrease in crystallite size. The result obtained from Ce^{3+} doped $Sr_2P_2O_7$ phosphors gives its potential use as a UV LED application.

- ❖ Eu^{3+} doped $Sr_2P_2O_7$ phosphor was excited under its major excitation wavelength of 396 and 466 nm. The PL emission occurs at 618 nm which is a red emission useful for LED applications. PL emission intensifications with increases in doping concentration, the maximum intensity of 618 nm emission peak for the 5.0 mol% Eu^{3+} is increased by 5-6 time than that of the 0.5 mol% Eu^{3+} . The PL emission also depends on the crystallite size, for Eu^{3+} doped $Sr_2P_2O_7$ phosphor the PL intensity increase with a decrease in crystallite size. The PL emission results of Eu^{3+} doped $Sr_2P_2O_7$ phosphor suggest its potential application for wLED under blue excitation.
- ❖ Tb^{3+} doped $Sr_2P_2O_7$ phosphor shows prominent emission of the Tb^{3+} transition under 323 nm excitation. It gives green emission under UV excitation. PL emission intensity of Tb^{3+} doped $Sr_2P_2O_7$ phosphor increases with doping concentration as well as the decrease in the crystallite size. Tb^{3+} doped $Sr_2P_2O_7$ phosphor is a good candidate for as a green phosphor under UV excitation.

4.4. Rare Earth co-doped Strontium Pyrophosphate

The photoluminescence properties of RE^{3+} co-doped $Sr_2P_2O_7$ phosphors were studied by taking 1.0 mol% Ce^{3+} as fixed dopant and 1.0 mol% Eu^{3+} , Tb^{3+} , Dy^{3+} , Er^{3+} , Gd^{3+} , Sm^{3+} as co-dopant. All RE^{3+} co-doped $Sr_2P_2O_7$ phosphors were synthesized by combustion method at heating temperature 1200°C. For the PL measurements, the phosphors were excited under different emission wavelength, and corresponds to the excitation spectra of the phosphors emission spectra were recorded for different excitation wavelength. Depending upon the splitting of the 5d excited state of Ce^{3+} ion by the crystal field symmetry, Ce^{3+} ion can be used as sensitizer as well as an activator in luminescence phosphor. in the majority of research work, Ce^{3+} ion is taken as a sensitizer, in which the energy transfer from Ce^{3+} ion to the different rare earth activator ions in different host lattice [7, 105]. In luminescent phosphor, energy transfer processes play important role in order to improve the PL emission efficiency, which can be accomplished by adding the impurity act as a sensitizer or transfer its energy to the other

atom or ion that can enhance luminescence efficiency. The process of energy transfer is called *sensitization of luminescence* [22].

4.4.1. $\text{Sr}_2\text{P}_2\text{O}_7$: Ce^{3+} , Eu^{3+}

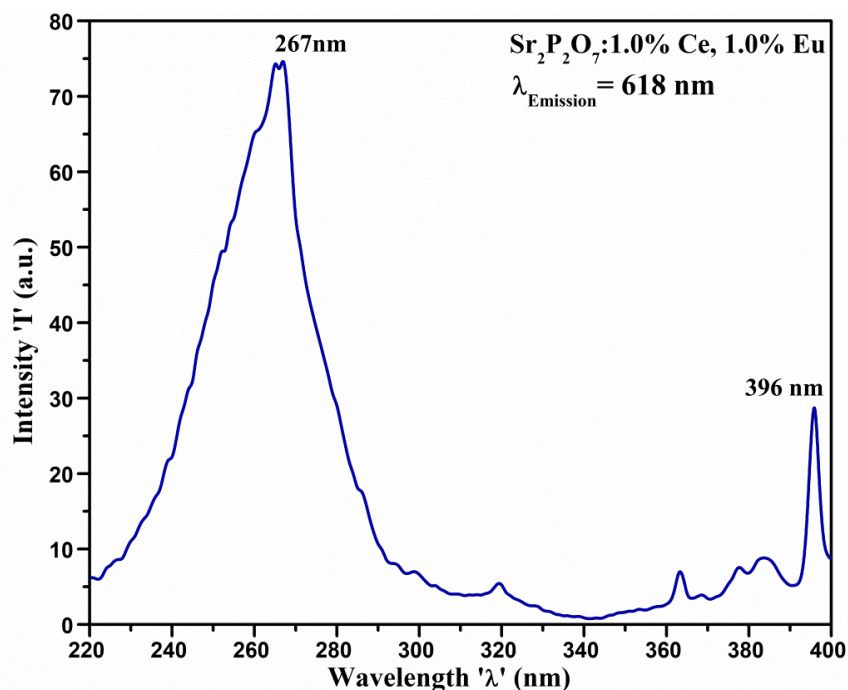


Figure 4.22 PL excitation spectra of 0.1mol% Ce^{3+} , 0.1mol% Eu^{3+} doped $\text{Sr}_2\text{P}_2\text{O}_7$ phosphor.

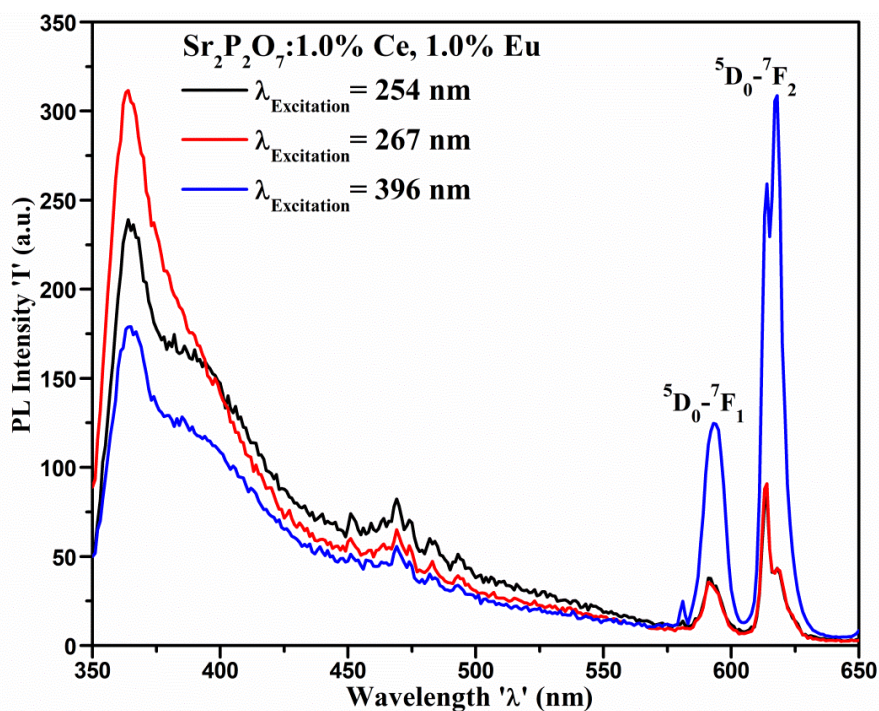


Figure 4.23 PL emission spectra of 1.0mol% Ce^{3+} , 1.0mol% Eu^{3+} doped $\text{Sr}_2\text{P}_2\text{O}_7$ phosphor.

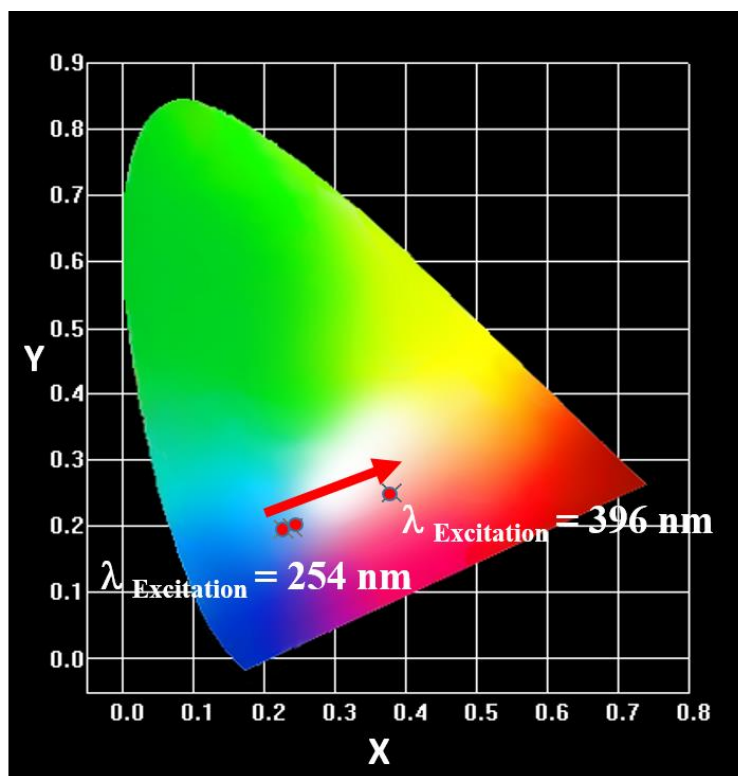


Figure 4.24 CIE chromaticity coordinate diagram of 0.1 mol% Ce^{3+} , 0.1 mol% Eu^{3+} doped $\text{Sr}_2\text{P}_2\text{O}_7$ phosphor.

Figure 4.22 shows the excitation spectra of Ce^{3+} - Eu^{3+} co-doped $\text{Sr}_2\text{P}_2\text{O}_7$ phosphors monitored at 618 nm emission wavelength. The excitation spectrum of the phosphor monitored at emission wavelength 618 nm consists of two broad bands centered at 267 nm and a small peak 396 nm. The broad peak centered at 267 nm is derived due to the $4f-5d$ transition of Ce^{3+} and small peak centered at 396 nm is derived due to the characteristic $4f-4f$ transitions of Eu^{3+} ion ascribed by the ${}^7\text{F}_0-{}^5\text{L}_6$ transition. It is reported that the energy transfer from Ce^{3+} ion to Eu^{3+} does not take place or very weak because Ce^{3+} ion having the lowest fourth ionization potential and Eu^{3+} ion having the highest third ionization potential in terms of the stability of completely- and half-filled shells [7, 106]. Figure 4.23 shows the PL emission spectra of Ce^{3+} - Eu^{3+} co-doped $\text{Sr}_2\text{P}_2\text{O}_7$ phosphors monitored at 254, 267 and 396 nm excitation wavelength. It is observed, the weak interaction between Ce^{3+} and Eu^{3+} causes the reduction in UV-blue emission of Ce^{3+} . Under 396 nm excitation, PL emission spectra show strong emission at 621 nm attributed to the ${}^5\text{D}_0-{}^7\text{F}_2$ characteristic transition of Eu^{3+} ion and at 595 nm is attributed to the ${}^5\text{D}_0-{}^7\text{F}_1$ transitions of Eu^{3+} ion [107, 108]. Under 254 and 276 nm excitation, PL emission due Ce^{3+} and Eu^{3+} reduced sharply may come about to the more

number of nonradiative transition take place at that excitation. Figure 4.24 shows the CIE chromaticity coordinates of Ce^{3+} , Eu^{3+} co-doped $\text{Sr}_2\text{P}_2\text{O}_7$ phosphor. Emission color CIE coordinates are $(X = 0.227, Y = 0.194)$, $(X = 0.239, Y = 0.197)$ and $(X = 0.380, Y = 0.251)$ for 254, 267 and 396 nm excitation wavelength respectively. It is found that the emission color shows a discrepancy from blue to red for low (254 nm) to high (396 nm) excitation wavelength. This indicates that Ce^{3+} , Eu^{3+} co-doped $\text{Sr}_2\text{P}_2\text{O}_7$ phosphor exhibits blue emission for 254 nm, 267 nm excitation and light red emission for 396 nm excitation.

4.4.2. $\text{Sr}_2\text{P}_2\text{O}_7: \text{Ce}^{3+}, \text{Tb}^{3+}$

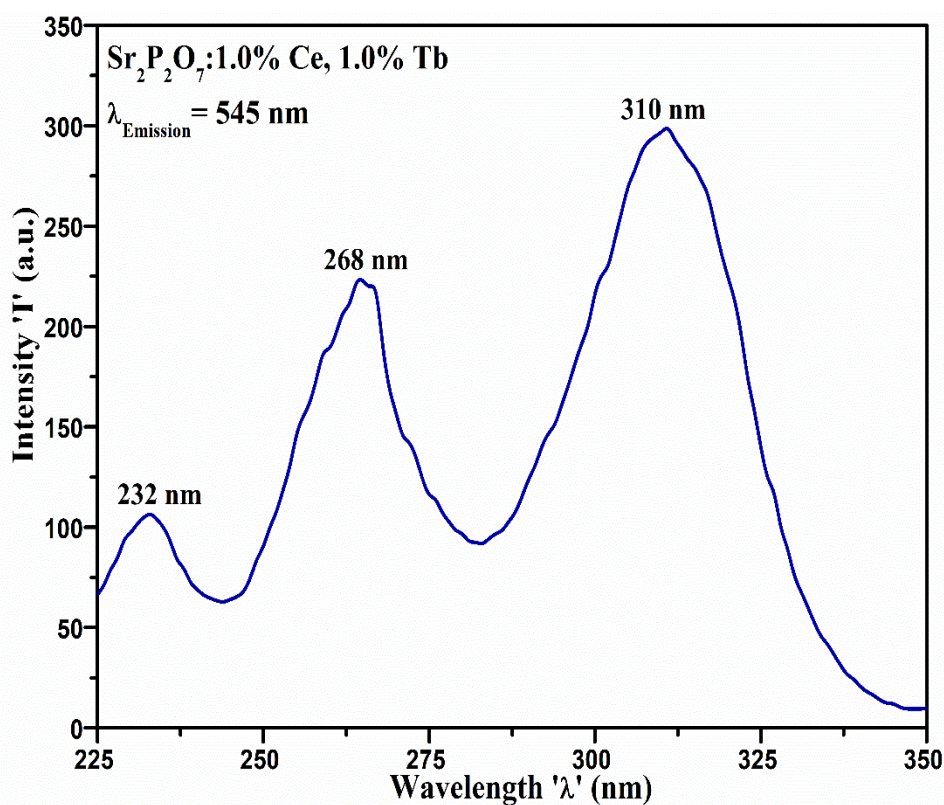


Figure 4.25 PL excitation spectra of 1.0mol% Ce^{3+} , 1.0mol% Tb^{3+} co-doped $\text{Sr}_2\text{P}_2\text{O}_7$ phosphor.

Figure 4.25 shows the excitation spectra of Ce^{3+} , Tb^{3+} co-doped $\text{Sr}_2\text{P}_2\text{O}_7$ monitored at 545 nm emission wavelength. In Figure 4.25, it is observed that the excitation spectrum of Ce^{3+} , Tb^{3+} co-doped $\text{Sr}_2\text{P}_2\text{O}_7$ exhibits an excitation peak at 232 nm corresponds to the $4f^8 - 4f^7 5d^1$ (f – d) electronic transitions of Tb^{3+} and two components with peaks positioned at 265 and 310 nm correspond to the crystal-field splitting of the excited 5d states of Ce^{3+} . There is only one electron in the 4f shell of Ce^{3+} ion that can be able to excite into the 5d orbitals. Although due to the crystal field splitting

and spin-orbit coupling of the excited 5d states, the excitation spectrum of Ce^{3+} reveals the direct splitting information of 5d orbital in the crystal field [109, 110].

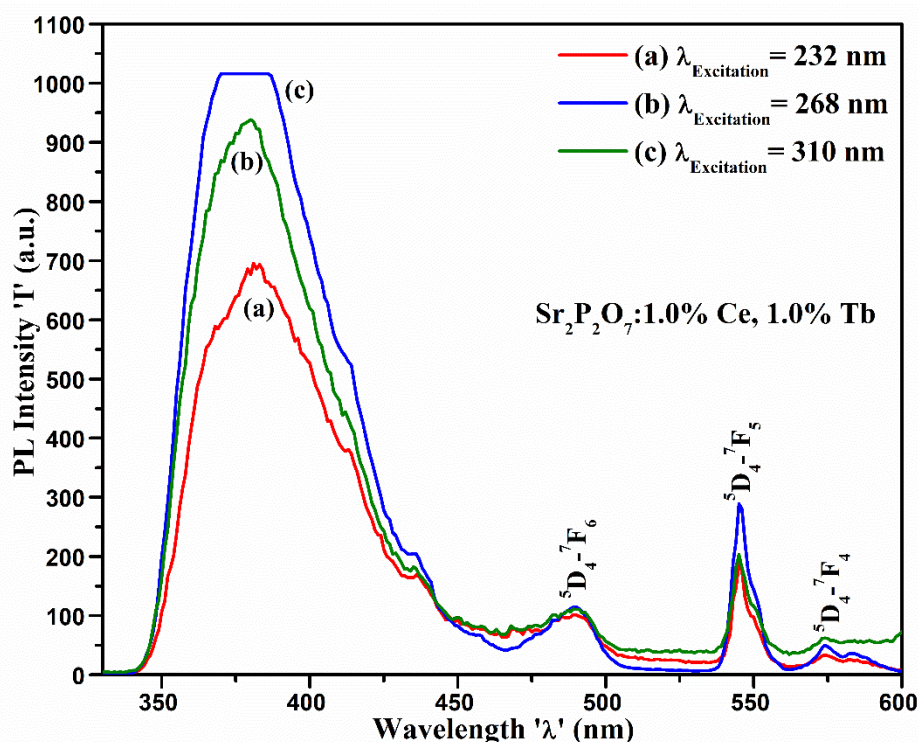


Figure 4.26 PL emission spectra of 0.1mol% Ce^{3+} , 0.1mol% Tb^{3+} doped $\text{Sr}_2\text{P}_2\text{O}_7$ phosphor.

To enhance the emission color of PL emission, the energy transfer process plays a vital role in solid-state luminescent phosphors. Electronic transitions of Tb^{3+} ion are strongly within $4f^n$ configurations that shows very appearance in the absorption spectra. Therefore, the energy transforming sensitizer ions with allowed electronic transition ions are added that absorb the excitation energy and transfer the energy to the activator ion. Ce^{3+} , Tb^{3+} co-doped $\text{Sr}_2\text{P}_2\text{O}_7$ phosphor, Ce^{3+} acts as sensitizer that transfer its absorbed energy to the Tb^{3+} activator and enhance the green emission. The energy levels of Tb^{3+} ion are significantly appropriate for the energy transfer process to take place from the allowed Ce^{3+} emission of (f-d) upon excitation with UV light. Figure 4.26 shows the emission spectra of Ce^{3+} , Dy^{3+} co-activated $\text{Sr}_2\text{P}_2\text{O}_7$ phosphors for different excitation wavelength. PL emission spectra show an intense UV-blue emission band and sharp emission line of characteristic transitions of Tb^{3+} ion for all three excitations. The sharp peaks centered at 491, 545 and 580 nm come about due to the characteristics radiative transitions of Tb^{3+} ion which can be attributed to the electron transitions $^5\text{D}_4-^7\text{F}_6$, $^5\text{D}_4-^7\text{F}_5$, and $^5\text{D}_4-^7\text{F}_4$, respectively. It is observed that the Ce^{3+} doping merge the $^5\text{D}_4-^7\text{F}_j$ ($J =$

3, 4, 5) electron transitions (shown in Figure 4.17) with blue emission of itself [111]. Maximum PL emission occurs under 268 nm excitation that recalled the maximum energy transfer takes place for that excitation.

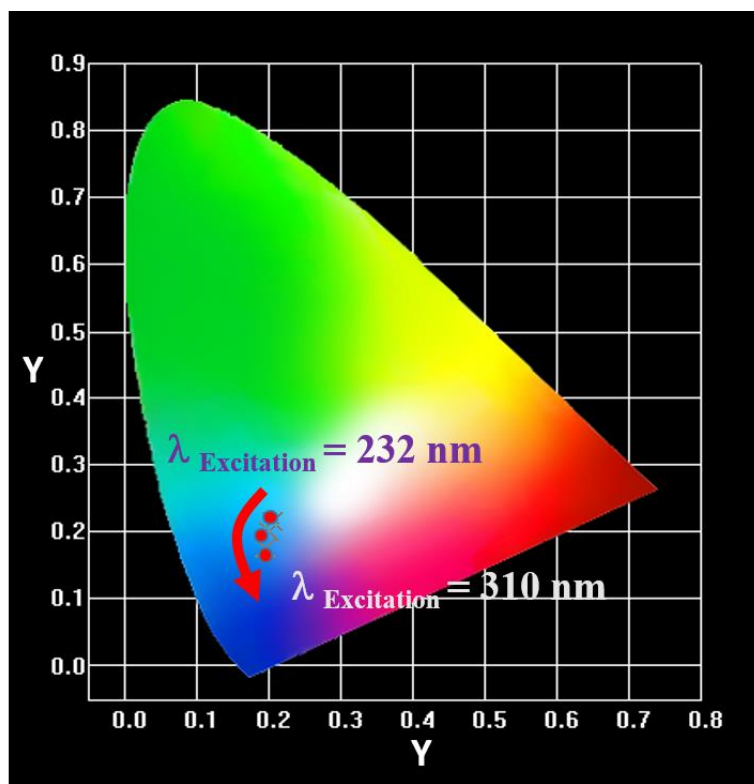


Figure 4.27 CIE chromaticity coordinate diagram of 0.1 mol% Ce^{3+} , 0.1 mol% Tb^{3+} -doped $\text{Sr}_2\text{P}_2\text{O}_7$ phosphor.

Figure 4.27 shows the CIE chromaticity coordinates of Ce^{3+} , Tb^{3+} co-doped $\text{Sr}_2\text{P}_2\text{O}_7$ phosphor. The calculated CIE coordinates of Ce^{3+} , Tb^{3+} co-doped $\text{Sr}_2\text{P}_2\text{O}_7$ phosphor are located in blue region, where blue color enhancement observed with the increment in excitation wavelength 232, 268 and 310 nm. CIE coordinates are ($X = 0.194$, $Y = 0.176$), ($X = 0.206$, $Y = 0.216$) and ($X = 0.201$, $Y = 0.200$) for 232, 268 and 310 nm excitation wavelength respectively. This indicates that Ce^{3+} , Tb^{3+} co-doped $\text{Sr}_2\text{P}_2\text{O}_7$ phosphor exhibits blue emission under UV excitation.

4.4.3. $\text{Sr}_2\text{P}_2\text{O}_7$: Ce^{3+} , Dy^{3+}

Figure 4.28 shows the excitation spectra of Ce^{3+} - Dy^{3+} co-doped $\text{Sr}_2\text{P}_2\text{O}_7$ phosphors monitored at 480 nm emission wavelength. The excitation spectrum of the phosphor comprises of two broad bands centered at 264 to 310 nm monitored at emission wavelength 480 nm which is derived from the $4f - 5d$ transition of Ce^{3+} . Figure 4.29 shows the emission spectra of Ce^{3+} , Dy^{3+} co-activated $\text{Sr}_2\text{P}_2\text{O}_7$ phosphors for different

excitation wavelength. The emission spectra obtained for three different excitation wavelengths shows different intensities with a similar shape.

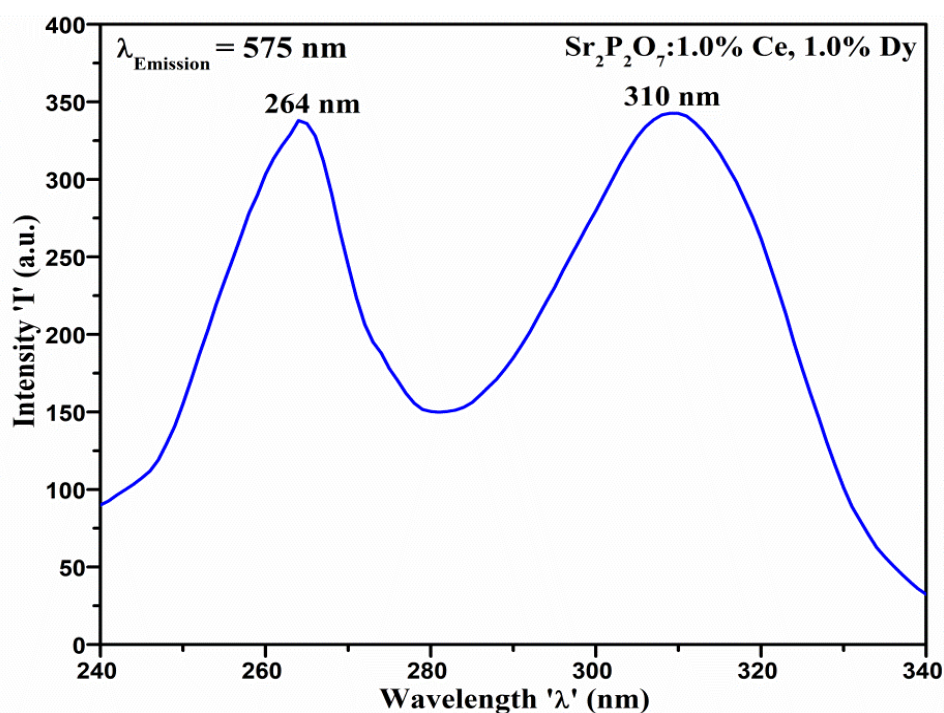


Figure 4.28 PL excitation spectra of 0.1mol% Ce³⁺, 0.1mol% Dy³⁺doped Sr₂P₂O₇ phosphor.

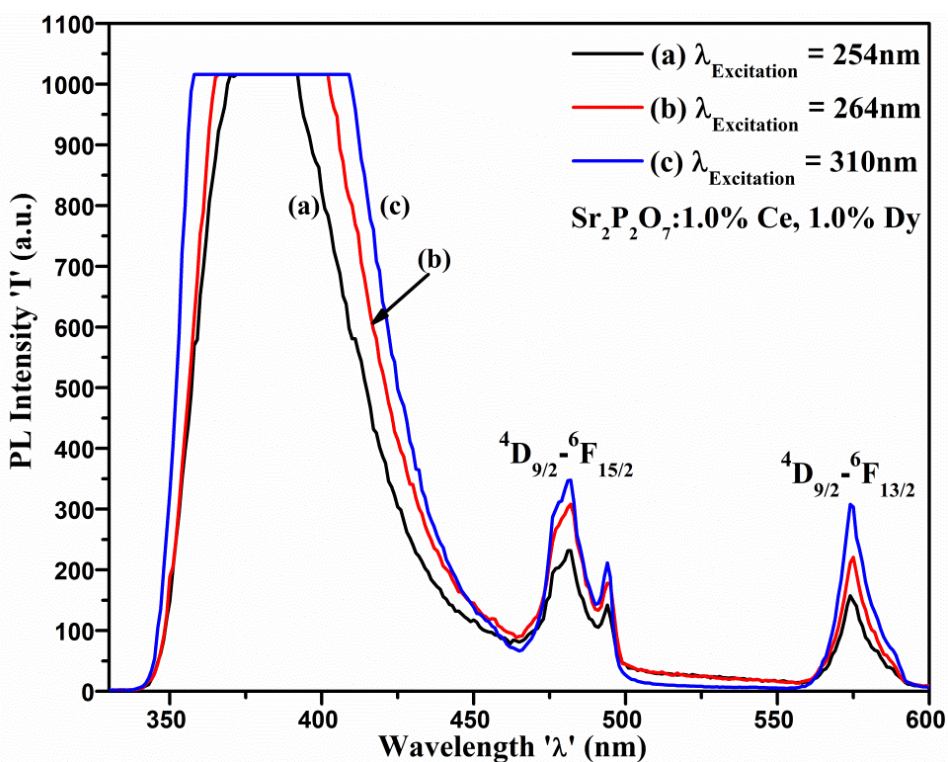


Figure 4.29 PL emission spectra of 1.0 mol% Ce³⁺, 1.0mol% Dy³⁺ doped Sr₂P₂O₇ phosphor.

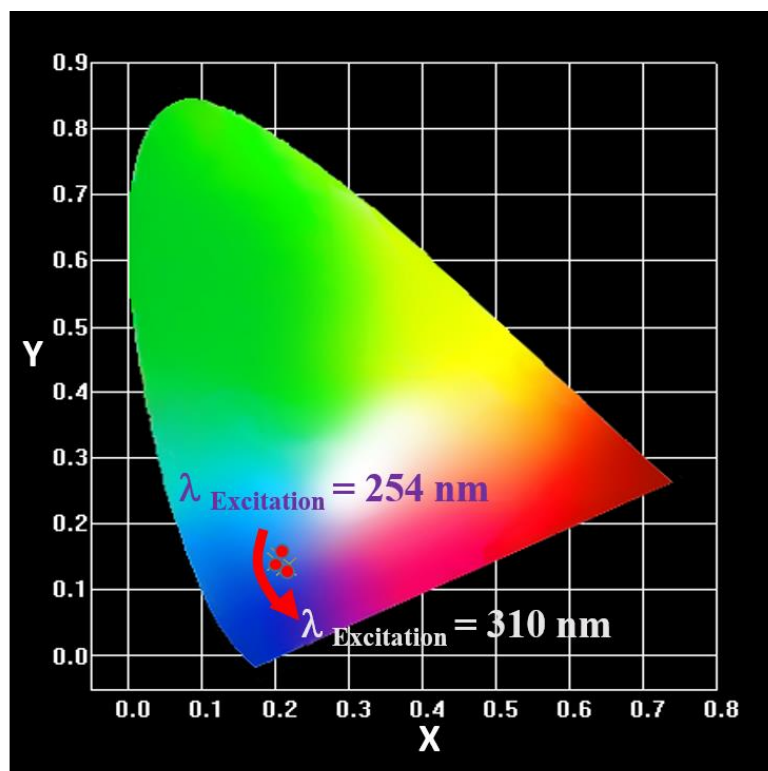


Figure 4.30 CIE chromaticity coordinate diagram of 0.1 mol% Ce^{3+} , 0.1 mol% Dy^{3+} doped $\text{Sr}_2\text{P}_2\text{O}_7$ phosphor.

As shown in Figure 4.29, when the $\text{Sr}_2\text{P}_2\text{O}_7$: 1.0% Ce^{3+} , 1.0% Dy^{3+} phosphor excited under 254, 264 and 310 nm wavelength, it shows three emission peaks at a wavelength around 380, 481 and 574 nm. Upon 254, 264 and 310 nm excitation, the phosphor exhibits emission due to the part of the excited Ce^{3+} ions is radiated to its ground state $^2\text{F}_{5/2}$ and $^2\text{F}_{7/2}$ through 380 nm emission band and the rest of energy of Ce^{3+} ions is transferred to the Dy^{3+} ions. Due to the absorption of energy, the Dy^{3+} ions is excited but it can decays to the metastable state $^4\text{F}_{9/2}$ through non-radiative transition and makes radiative emission transitions through $^4\text{F}_{9/2} \rightarrow ^6\text{H}_{15/2}$ (481 nm) and $^4\text{F}_{9/2} \rightarrow ^6\text{H}_{13/2}$ (574 nm) [112]. $\text{Sr}_2\text{P}_2\text{O}_7$ exhibits strong emission bands with maximum intensity at 390 nm analogous to the combined effect of transitions from the 5d excited state to $^2\text{F}_{5/2}$ and $^2\text{F}_{7/2}$ low-energy states of Ce^{3+} , respectively. In emission spectra, it can be found that the intensity of emission peak centered at 380 nm increase with decreasing the excitation energy. The maximum emission intensity occurs at excitation wavelength of 310 nm. The asymmetric emission band centered at 390 nm is induced due to the spin-orbit coupled into two levels of ground state of Ce^{3+} . As the intensities of the emission band are very high (out of scale), it is not convenient to find the two peak by Gaussian peak

fitting. But the result is significant with the Ce^{3+} doped $\text{Sr}_2\text{P}_2\text{O}_7$ phosphor as shown in Figure 4.7, where the emission band induced due to the spin-orbit splitting of the 4f ground state with energy difference about 2081 cm^{-1} , which agrees with the theoretical value 2000 cm^{-1} [3]. The emission spectra also contains two sharp peaks centered at 481 nm and 574 nm. The blue emission at 481 nm is attributed to the magnetic dipole transition of $^4\text{F}_{9/2} - ^6\text{H}_{15/2}$, the yellow emission at 574 nm is related to the electric dipole transition of $^4\text{F}_{9/2} - ^6\text{H}_{13/2}$ of Dy^{3+} ion [113]. The emission of Dy^{3+} located at 481 nm and 574 nm is executed by Ce^{3+} ion which can be attributed to the energy transfer occur from the Ce^{3+} ion to the Dy^{3+} ion in the $\text{Sr}_2\text{P}_2\text{O}_7$ phosphor. Figure 4.30 shows the CIE chromaticity coordinates of Ce^{3+} , Dy^{3+} co-doped $\text{Sr}_2\text{P}_2\text{O}_7$ phosphor. The calculated CIE coordinates of Ce^{3+} , Dy^{3+} co-doped $\text{Sr}_2\text{P}_2\text{O}_7$ phosphor are situated in the blue region, where blue color enhancement observed with the increment in excitation wavelength 232, 268 and 310 nm. CIE coordinates are $(X = 0.208, Y = 0.150)$, $(X = 0.203, Y = 0.142)$ and $(X = 0.214, Y = 0.136)$ for 254, 268 and 310 nm excitation wavelength respectively. This indicates that Ce^{3+} , Dy^{3+} co-doped $\text{Sr}_2\text{P}_2\text{O}_7$ phosphor exhibits blue emission under UV excitation.

4.4.4. $\text{Sr}_2\text{P}_2\text{O}_7$: Ce^{3+} , Sm^{3+}

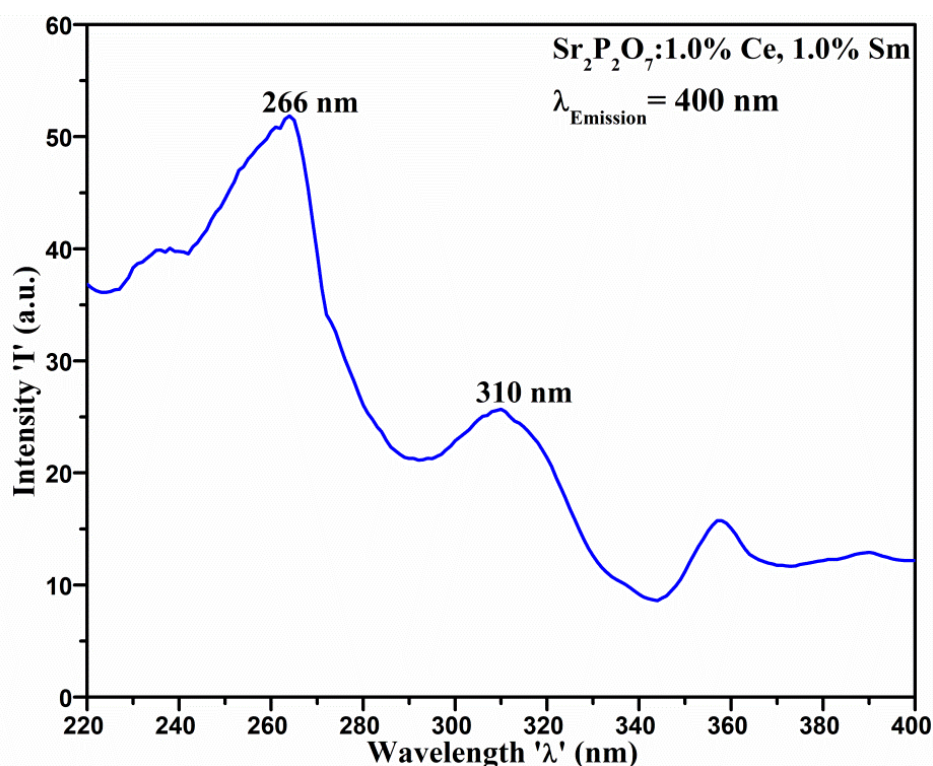


Figure 4.31 PL excitation spectra of 0.1mol% Ce^{3+} , 0.1mol% Sm^{3+} doped $\text{Sr}_2\text{P}_2\text{O}_7$ phosphor.

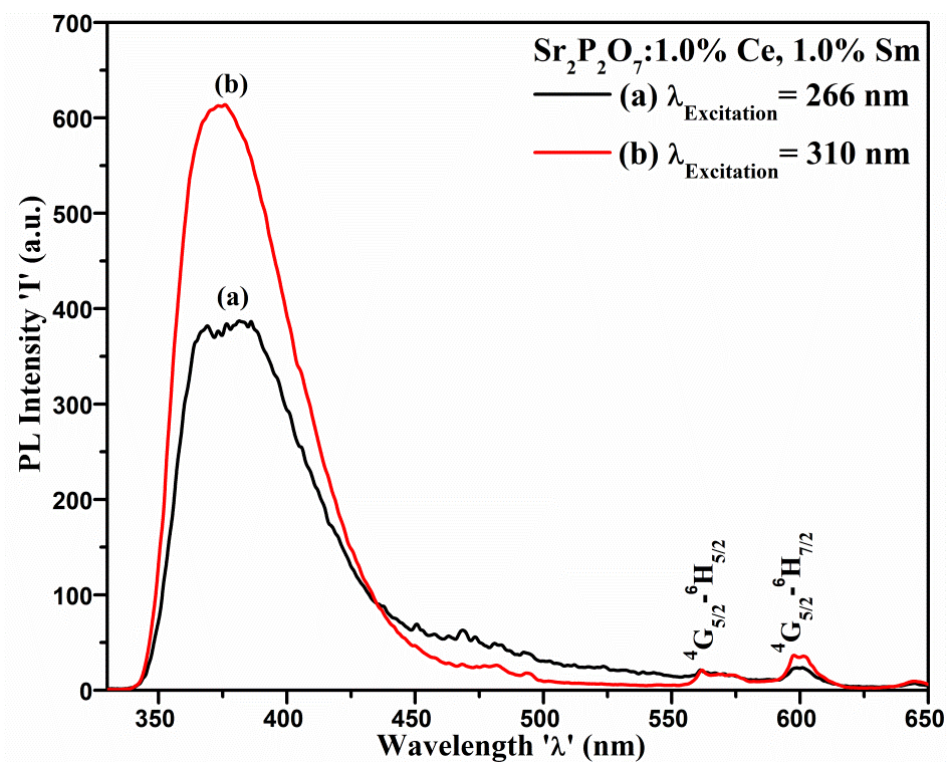


Figure 4.32 PL emission Spectra of 0.1mol% Ce³⁺, 0.1mol% Sm³⁺doped Sr₂P₂O₇ phosphor.

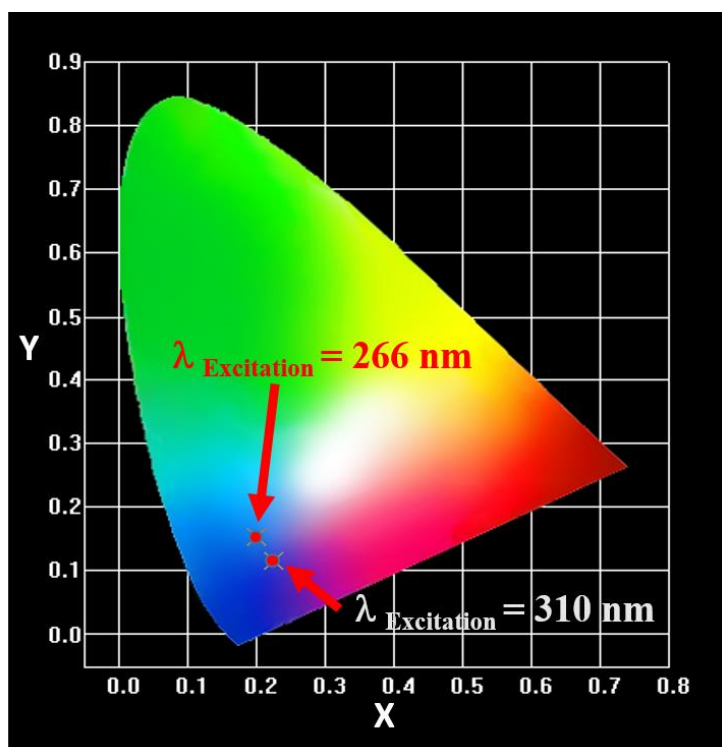


Figure 4.33 CIE chromaticity coordinate diagram of 0.1mol% Ce³⁺, 0.1mol% Sm³⁺doped Sr₂P₂O₇ phosphor.

Figure 4.31 shows the excitation of Ce^{3+} - Sm^{3+} co-doped $\text{Sr}_2\text{P}_2\text{O}_7$ monitored at 400 nm emission wavelength. The excitation spectra contain two absorption bands centered at 266 nm and 310 nm ascribe to the $4f - 5d$ transition of Ce^{3+} ion. The excitation spectra extended up to 400 nm because of multiple $f - f$ transition of Sm^{3+} ion. Figure 4.32 shows PL emission spectra of Ce^{3+} - Sm^{3+} co-doped $\text{Sr}_2\text{P}_2\text{O}_7$ monitored at 266 and 310 nm excitation wavelength. From the figure, it is found that the excitation spectra and emission spectra overlapped which resulting due to the energy transfer phenomenon can occur from Ce^{3+} to Sm^{3+} ions in host $\text{Sr}_2\text{P}_2\text{O}_7$. PL emission spectra of Ce^{3+} , Sm^{3+} doped $\text{Sr}_2\text{P}_2\text{O}_7$ consist of broad emission band ranging from 345 – 450 nm and two solder peak centered at 565 nm and 599 nm. Broad emission band formation resulting due to the part of the excited Ce^{3+} ions is radiated to its ground state $^2\text{F}_{5/2}$ and $^2\text{F}_{7/2}$ through emission band centered at 380 nm and formation of small characteristic emission peak at 565 nm and 599 nm resulting due to transition $^4\text{G}_{5/2} - ^6\text{H}_{5/2}$ and $^4\text{G}_{5/2} - ^6\text{H}_{7/2}$, respectively. PL emission spectra illustrate the emission due to Ce^{3+} is much stronger than that of the emission due to Sm^{3+} . This came about because of more number of Sr^{2+} site has been substituted by Ce^{3+} ions rather than Sm^{3+} ions, as a result, a small amount of energy transformation occurs from Ce^{3+} to Sm^{3+} ion. PL emission spectra show the intensity of the PL emission reduced for higher excitation energy at excitation wavelength 266 nm. In higher excitation majority energy is dissipated by a nonradiative transition which can reduce the population of a radiative electron in an excited state and minimize the radiative transitions. At low excitation energy, the percentage of nonradiative transition compare to the radiative transition is miniature which results into high PL emission. CIE chromaticity coordinates of PL emission of Ce^{3+} - Sm^{3+} co-doped $\text{Sr}_2\text{P}_2\text{O}_7$ monitored at 266 nm and 310 nm are $(X = 0.201, Y = 0.353)$ and $(X = 0.225, Y = 0.114)$ respectively. CIE chromaticity coordinates diagram of Ce^{3+} - Sm^{3+} co-doped $\text{Sr}_2\text{P}_2\text{O}_7$ is shown in Figure 4.33. It is noted that the CIE chromaticity coordinates for different excitation located in the blue region of color coordinate, where the emission due to 310 nm excitation wavelength is shifted toward the UV-violet color. Thus the synthesized Ce^{3+} - Sm^{3+} co-doped $\text{Sr}_2\text{P}_2\text{O}_7$ is a potential blue phosphor under UV excitation.

4.4.5. $\text{Sr}_2\text{P}_2\text{O}_7$: Ce^{3+} , Er^{3+}

Figure 4.34 shows the excitation of Ce^{3+} , Er^{3+} co-doped $\text{Sr}_2\text{P}_2\text{O}_7$ monitored at 400 nm emission wavelength of Ce^{3+} , Gd^{3+} co-doped $\text{Sr}_2\text{P}_2\text{O}_7$. The excitation spectra contain two

absorption bands centered at 266 nm and 310 nm ascribe to the $4f - 5d$ transition of Ce^{3+} ion.

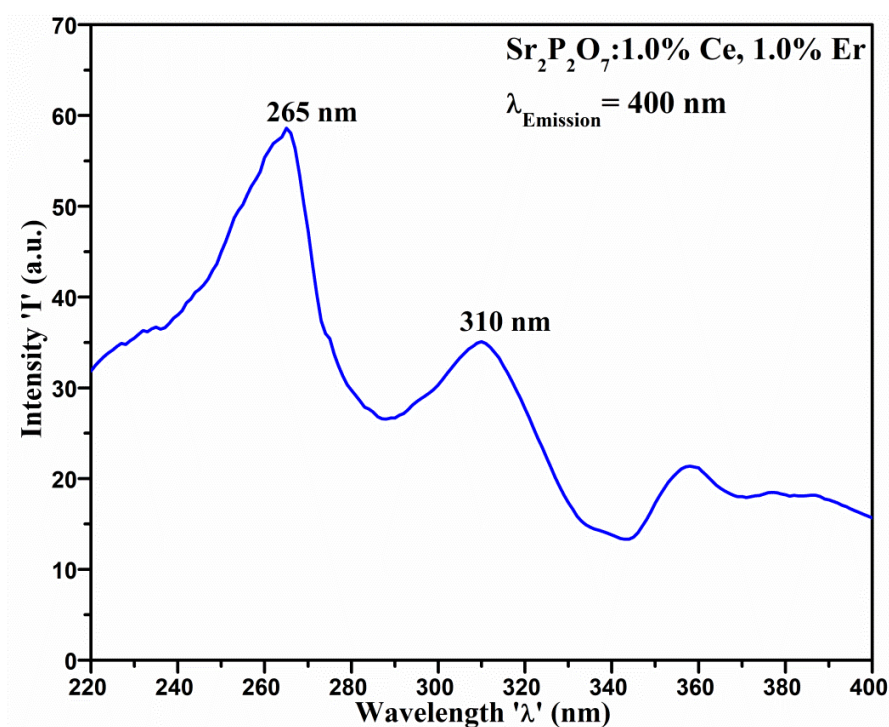


Figure 4.34 PL excitation Spectra of 0.1mol% Ce^{3+} , 0.1mol% Er^{3+} doped $Sr_2P_2O_7$ phosphor.

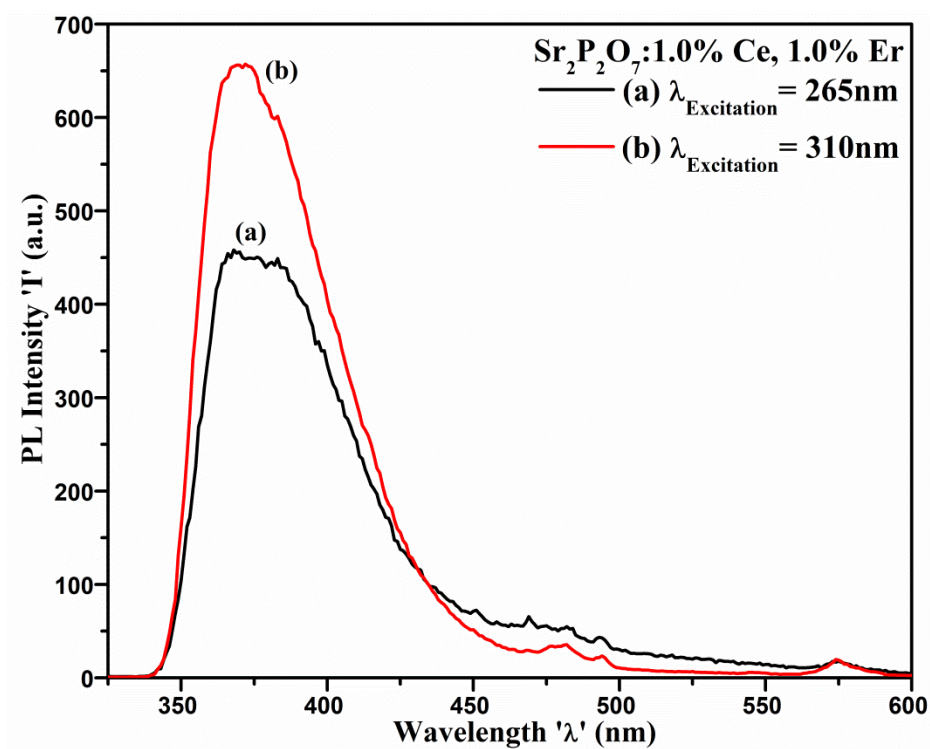


Figure 4.35 PL emission spectra of 0.1mol% Ce^{3+} , 0.1mol% Er^{3+} doped $Sr_2P_2O_7$ phosphor.

Figure 4.34 shows the excitation of Ce^{3+} , Er^{3+} co-doped $\text{Sr}_2\text{P}_2\text{O}_7$ monitored at 268 and 310 nm emission wavelength. Under two excitation wavelength, PL emission takes place in the UV-blue region due to the transition of Ce^{3+} ion and little bit emission of Er^{3+} . Figure 4.35 shows PL emission spectra of Ce^{3+} - Er^{3+} co-doped $\text{Sr}_2\text{P}_2\text{O}_7$ monitored at 265 and 310 nm excitation wavelength. The incorporation of Er^{3+} ions into the host lattice site does not improve its own emission and no energy transfer occur between Ce^{3+} to the Er^{3+} . The interaction between Ce^{3+} and Er^{3+} ion is negligible for the given phosphor, therefore the emission of Ce^{3+} ion remains unaffected after co-doping with Er^{3+} [114, 115]. The calculated values of CIE coordinates of emission color Ce^{3+} , Er^{3+} co-doped $\text{Sr}_2\text{P}_2\text{O}_7$ phosphor to be found in the violet region for both excitation wavelength 265 and 310 nm. CIE coordinates are $(X = 0.279, Y = 0.160)$ and $(X = 0.271, Y = 0.162)$ for 268 and 310 nm excitation wavelength respectively. This indicates that Ce^{3+} , Er^{3+} co-doped $\text{Sr}_2\text{P}_2\text{O}_7$ phosphor exhibits near UV-violet emission under UV excitation which gives its potential application for UV LED phosphor.

4.4.6. $\text{Sr}_2\text{P}_2\text{O}_7: \text{Ce}^{3+}, \text{Gd}^{3+}$

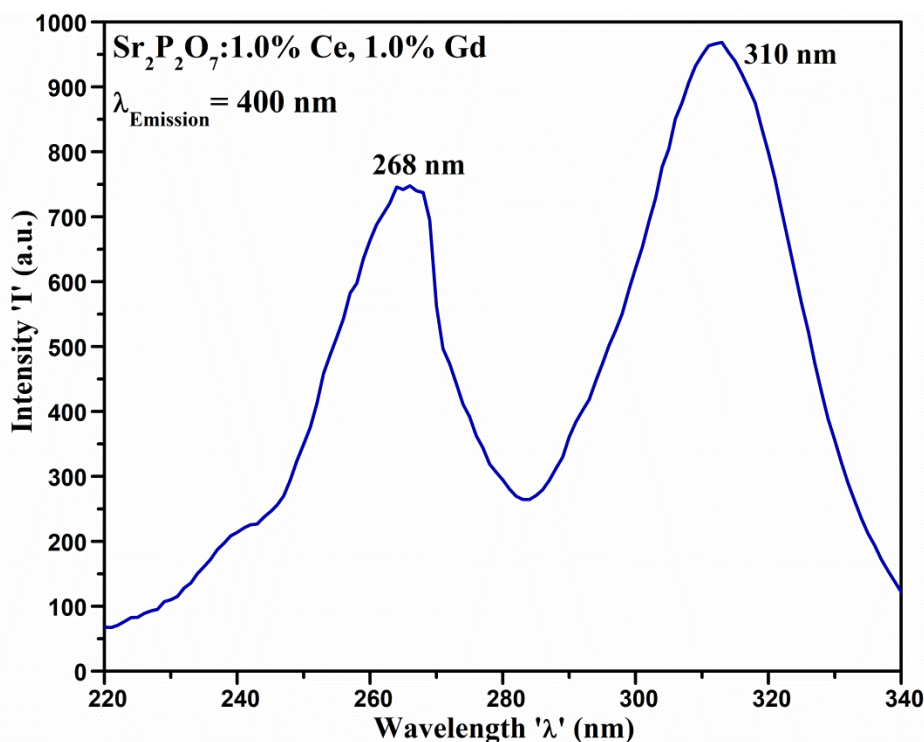


Figure 4.36 PL excitation spectra of 0.1 mol% Ce^{3+} , 0.1 mol% Gd^{3+} doped $\text{Sr}_2\text{P}_2\text{O}_7$ phosphor.

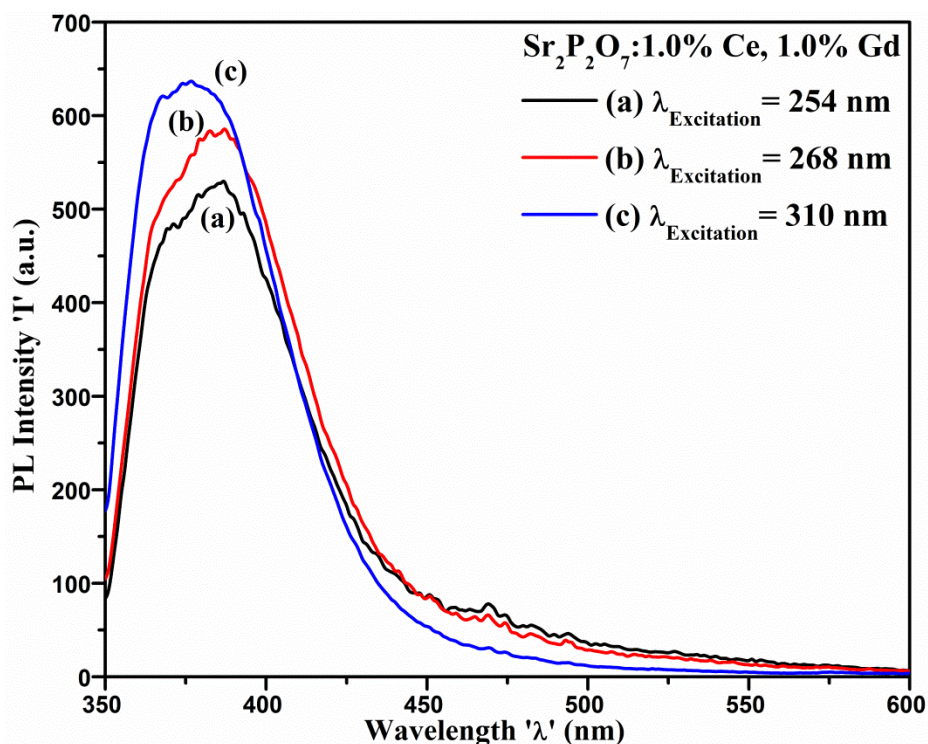


Figure 4.37 PL emission spectra of 0.1 mol% Ce³⁺, 0.1 mol% Gd³⁺doped Sr₂P₂O₇ phosphor.

Figure 4.36 shows the excitation of Ce³⁺, Gd³⁺ co-doped Sr₂P₂O₇ monitored at 400 nm emission wavelength. The excitation spectra contain two absorption bands centred at 266 nm and 310 nm ascribe to the 4f – 5d transition of Ce³⁺ ion. **Figure 4.37** shows the excitation of Ce³⁺, Gd³⁺ co-doped Sr₂P₂O₇ monitored at 254, 268 and 310 nm emission wavelength. Doping of Gd³⁺ cannot induce the PL emission due to zero sensitizing effect between Ce³⁺ and Gd³⁺. The calculated CIE coordinates situated of Ce³⁺, Gd³⁺ co-doped Sr₂P₂O₇ phosphor in blue region, where blue color enhancement observed with the increment in excitation wavelength 232, 268 and 310 nm. CIE coordinates are (X = 0.275, Y = 0.164), (X = 0.279, Y = 0.160) and (X = 0.271, Y = 0.162) for 254, 268 and 310 nm excitation wavelength respectively. This indicates that Ce³⁺, Gd³⁺ co-doped Sr₂P₂O₇ phosphor exhibits blue emission under UV excitation.

Photoluminescence Output of RE³⁺ co-doped Sr₂P₂O₇

The photoluminescence studies for RE³⁺ co-doped Sr₂P₂O₇ phosphors displayed fascinating results, the following are the logical conclusions:

- ❖ 1.0 mol% Ce³⁺, 1.0 mol% Eu³⁺ doped Sr₂P₂O₇ phosphor shows a prominent 618 nm red emission under the excitation wavelength 396 nm. The emission under the

excitation wavelength 254 and 268 nm show weak emission due to the weak interaction between the Ce^{3+} and Eu^{3+} ions. Therefore, Eu^{3+} reduces Ce^{3+} emission. This phosphor gives light red emission under 396 nm excitation.

- ❖ 1.0 mol% Ce^{3+} , 1.0 mol% Tb^{3+} doped $\text{Sr}_2\text{P}_2\text{O}_7$ phosphor shows prominent 395 nm UV emission under the excitation wavelength 232, 268 and 310 nm. The emission peak observed at 545 nm is occur due to the incorporation of Tb^{3+} ion in the host. There is a small amount of sensitizing occurs between Ce^{3+} and Tb^{3+} ions. Due to the combined effect of Ce^{3+} and Tb^{3+} , the emission color obtained in the UV-Blue region of CIE diagram.
- ❖ 1.0 mol% Ce^{3+} , 1.0 mol% Dy^{3+} doped $\text{Sr}_2\text{P}_2\text{O}_7$ phosphor shows prominent 395 nm UV emission which is out of scale under the excitation wavelength 254, 264 and 310 nm. The emission occur due to allowed electron transition of Dy^{3+} are observed at 481 nm and 574 nm. The observation suggests that there is an energy transfer process occur between Ce^{3+} and Dy^{3+} , which arise due to the co-coping in the phosphor.
- ❖ 1.0 mol% Ce^{3+} doped with 1.0 mol% Sm^{3+} , Er^{3+} , and Gd^{3+} did not give emission except the basic Ce^{3+} emission around at 395 nm as observed in RE^{3+} doping. This could occur due to the nonradiative transitions of Sm^{3+} , Er^{3+} , and Gd^{3+} .

References

1. Danielson, E., et al., *A combinatorial approach to the discovery and optimization of luminescent materials*. Nature, 1997. **389**(6654): p. 944.
2. Ronda, C.R., *Emission and excitation mechanisms of phosphors*, 2007: Wiley Online Library.
3. Blasse, G. and B. Grabmaier, *Luminescent materials*, 2012: Springer Science & Business Media.
4. Feldmann, C., et al., *Inorganic luminescent materials: 100 years of research and application*. Advanced Functional Materials, 2003. **13**(7): p. 511-516.
5. Schulman, J.H., R.J. Ginther, and C.C. Klick, *A study of the mechanism of sensitized luminescence of solids*. Journal of the Electrochemical Society, 1950. **97**(4): p. 123-132.
6. Shinde, K.N., et al., *Basic mechanisms of photoluminescence*, in *Phosphate Phosphors for Solid-State Lighting*, 2012, Springer. p. 41-59.

7. Blasse, G., *Chemistry and physics of R-activated phosphors*. Handbook on the physics and chemistry of rare earths, 1979. **4**: p. 237-274.
8. Hercules, D.M., *Fluorescence and phosphorescence analysis: principles and applications*. Fluorescence and Phosphorescence Analysis: Principles and Applications/Ed. David M. Hercules. New York, NY: Interscience Publishers, 1966.
9. Lichtman, J.W. and J.-A. Conchello, *Fluorescence microscopy*. Nature methods, 2005. **2**(12): p. 910.
10. Cid, M.-M. and J. Bravo, *Structure Elucidation in Organic Chemistry: The Search for the Right Tools*, 2014: John Wiley & Sons.
11. Bernath, P.F., *Spectra of atoms and molecules*, 2015: Oxford University Press.
12. Svanberg, S., *Atomic and molecular spectroscopy: basic aspects and practical applications*. Vol. 6. 2012: Springer Science & Business Media.
13. Goldberg, P.G., *Luminescence of inorganic solids*. 1966.
14. Jabłoński, A., *Über den mechanismus der photolumineszenz von farbstoffphosphoren*. Zeitschrift für Physik, 1935. **94**(1-2): p. 38-46.
15. Jelley, E.E., *Spectral absorption and fluorescence of dyes in the molecular state*. Nature, 1936. **138**(3502): p. 1009.
16. Wasserberg, D., *Triplet states-triplet fates: phosphorescence and energy transfer in functional molecules*. 2006.
17. Gilbert, A. and J.E. Baggott, *Essentials of molecular photochemistry*, 1991: CRC.
18. Turro, N.J., *Modern molecular photochemistry*, 1991: University science books.
19. Li, L., et al., *Atomic and Molecular Low-n Rydberg States in Near Critical Point Fluids*, in *Advanced Aspects of Spectroscopy*, 2012, InTech.
20. Leverenz, H.W. and F. Urbach, *Introduction to the Luminescence of Solids*. Physics Today, 1950. **3**: p. 32.
21. Khalid, A.H. and K. Kontis, *Thermographic phosphors for high temperature measurements: principles, current state of the art and recent applications*. Sensors, 2008. **8**(9): p. 5673-5744.
22. Shionoya, S., W.M. Yen, and H. Yamamoto, *Phosphor handbook*, 2006: CRC press.
23. Yen, W.M. and H. Yamamoto, *Fundamentals of phosphors*, 2006: CRC press.
24. So, P.T. and C.Y. Dong, *Fluorescence spectrophotometry*. eLS, 2002.

25. Lakowicz, J.R., *Principles of Fluorescence Spectroscopy*, (1999), 2004, Kluwer Academic/Plenum Publishers, New York.
26. Becker, R.S., *Theory and interpretation of fluorescence and phosphorescence*. 1969.
27. Berezin, M.Y. and S. Achilefu, *Fluorescence lifetime measurements and biological imaging*. Chemical reviews, 2010. **110**(5): p. 2641-2684.
28. Lippert, E., *N. Mataga und T. Kubota: Molecular Interactions and Electronic Spectra*. Marcel Dekker, Inc., New York, 1970, Seiten. Berichte der Bunsengesellschaft für physikalische Chemie, 1971. **75**(6): p. 603-603.
29. Widengren, J. and P. Schwille, *Characterization of photoinduced isomerization and back-isomerization of the cyanine dye by fluorescence correlation spectroscopy*. The Journal of Physical Chemistry A, 2000. **104**(27): p. 6416-6428.
30. Sauer, M., J. Hofkens, and J. Enderlein, *Basic principles of fluorescence spectroscopy*. Handbook of fluorescence spectroscopy and imaging: from single molecules to ensembles, 2011: p. 1-30.
31. Vogt Jr, R., G. Marti, and V. Zenger, *Standardization and quality assurance in fluorescence measurements I*. Resch-Genger Ed.) Springer Berlin Heidelberg, 2008. **5**: p. 3-31.
32. Patterson, G.H. and D.W. Piston, *Photobleaching in two-photon excitation microscopy*. Biophysical journal, 2000. **78**(4): p. 2159-2162.
33. Waynant, R.W. and M.N. Ediger, *Electro-optics handbook*, 2000: McGraw-Hill New York.
34. Kleppner, D., *Inhibited spontaneous emission*. Physical Review Letters, 1981. **47**(4): p. 233.
35. Toro, C., *Polarization Dependent Two-photon Absorption Properties Of Chiral Molecules*. 2010.
36. Solé, J., L. Bausa, and D. Jaque, *An introduction to the optical spectroscopy of inorganic solids*, 2005: John Wiley & Sons.
37. Tanner, P.A., *Some misconceptions concerning the electronic spectra of tri-positive europium and cerium*. Chemical Society Reviews, 2013. **42**(12): p. 5090-5101.

38. Harris, D.C. and M.D. Bertolucci, *Symmetry and spectroscopy: an introduction to vibrational and electronic spectroscopy*, 1978: Courier Corporation.
39. Valeur, B. and M.N. Berberan-Santos, *Molecular fluorescence: principles and applications*, 2012: John Wiley & Sons.
40. De Sa, G., et al., *Spectroscopic properties and design of highly luminescent lanthanide coordination complexes*. Coordination Chemistry Reviews, 2000. **196**(1): p. 165-195.
41. Sharma, A. and S.G. Schulman, *Introduction to fluorescence spectroscopy*. Vol. 13. 1999: Wiley-interscience.
42. Steigerwald, D.A., et al., *Illumination with solid state lighting technology*. IEEE journal of selected topics in quantum electronics, 2002. **8**(2): p. 310-320.
43. Rohwer, L.S. and A.M. Srivastava, *Development of Phosphors for LEDs*. Electrochem. Soc. Interface, 2003. **12**(2): p. 36-39.
44. Sheu, J.-K., et al., *Warm-white light-emitting diode with high color rendering index fabricated by combining trichromatic InGaN emitter with single red phosphor*. Optics express, 2015. **23**(7): p. A232-A239.
45. Murthy, K., *Nano phosphors for light emitting diodes (LEDs) Syntheses and Characterization*. Recent Research in Science and Technology, 2012. **4**(8).
46. Muthu, S., F.J. Schuurmans, and M.D. Pashley, *Red, green, and blue LEDs for white light illumination*. IEEE Journal of selected topics in quantum electronics, 2002. **8**(2): p. 333-338.
47. Smet, P.F., A.B. Parmentier, and D. Poelman, *Selecting conversion phosphors for white light-emitting diodes*. Journal of the Electrochemical Society, 2011. **158**(6): p. R37-R54.
48. Lister, G.G., et al., *The physics of discharge lamps*. Reviews of modern physics, 2004. **76**(2): p. 541.
49. Safari, S., et al., *Ultraviolet radiation emissions and illuminance in different brands of compact fluorescent lamps*. International Journal of Photoenergy, 2015. **2015**.
50. Ronda, C.R., *Luminescence: from theory to applications*, 2007: John Wiley & Sons.
51. Höpfe, H.A., *Recent developments in the field of inorganic phosphors*. Angewandte Chemie International Edition, 2009. **48**(20): p. 3572-3582.

52. Greskovich, C. and S. Duclos, *Ceramic scintillators*. Annual review of materials science, 1997. **27**(1): p. 69-88.
53. Yanagida, T., *Inorganic scintillating materials and scintillation detectors*. Proceedings of the Japan Academy, Series B, 2018. **94**(2): p. 75-97.
54. Lecoq, P., A. Gektin, and M. Korzhik, *Inorganic scintillators for detector systems: physical principles and crystal engineering*, 2016: Springer.
55. Lecoq, P., *Development of new scintillators for medical applications*. Nuclear Instruments and Methods in Physics Research Section A: Accelerators, Spectrometers, Detectors and Associated Equipment, 2016. **809**: p. 130-139.
56. Nakajima, T., B. Žemva, and A. Tressaud, *Advanced inorganic fluorides: synthesis, characterization and applications*, 2000: Elsevier.
57. Van Eijk, C.W., *Inorganic scintillators in medical imaging*. Physics in Medicine & Biology, 2002. **47**(8): p. R85.
58. Xu, R. and Y. Xu, *Modern inorganic synthetic chemistry*, 2010: Elsevier.
59. Ronda, C., T. Jüstel, and H. Nikol, *Rare earth phosphors: fundamentals and applications*. Journal of Alloys and Compounds, 1998. **275**: p. 669-676.
60. Chen, G., et al., *Upconversion nanoparticles: design, nanochemistry, and applications in theranostics*. Chemical reviews, 2014. **114**(10): p. 5161-5214.
61. Medishetty, R., et al., *Nonlinear optical properties, upconversion and lasing in metal–organic frameworks*. Chemical Society Reviews, 2017. **46**(16): p. 4976-5004.
62. Ronda, C., et al., *Luminescent Materials, Biological Applications*. Encyclopedia of Industrial Biotechnology: Bioprocess, Bioseparation, and Cell Technology, 2009: p. 1-13.
63. Murthy, K., *Up-conversion phosphors synthesis and application in solar converters*. Journal ISSN No, 2013. **2277**: p. 6362.
64. Chen, X., et al., *Photon upconversion in core–shell nanoparticles*. Chemical Society Reviews, 2015. **44**(6): p. 1318-1330.
65. Mondal, P.P. and A. Diaspro, *Fundamentals of fluorescence microscopy: exploring life with light*, 2013: Springer Science & Business Media.
66. Svoboda, K. and R. Yasuda, *Principles of two-photon excitation microscopy and its applications to neuroscience*. Neuron, 2006. **50**(6): p. 823-839.

67. Hou, D., et al., *Luminescence of Ce³⁺ at two different sites in α -Sr₂P₂O₇ under vacuum ultraviolet-UV and x-ray excitation*. Journal of Applied Physics, 2010. **108**(8): p. 083527.
68. Chen, M., Z. Xia, and Q. Liu, *Luminescence properties and energy transfer of Ce³⁺/Tb³⁺ co-doped Ca₆Ba (PO₄)₄O phosphor for near-UV pumped light-emitting diodes*. Journal of Materials Chemistry C, 2015. **3**(16): p. 4197-4204.
69. Li, M.R., et al., *Low-Temperature Flux Synthesis, Crystal Structure and Ce-Doped Luminescence of the First Lutetium Diphosphate NH₄LuP₂O₇*. European journal of inorganic chemistry, 2005. **2005**(23): p. 4693-4696.
70. Wisniewski, D., et al., *Scintillation and luminescence properties of Ce-activated K₃Lu (PO₄)₂*. Journal of alloys and compounds, 2004. **380**(1-2): p. 191-195.
71. Liu, R.-S., *Phosphors, up conversion nano particles, quantum dots and their applications*, 2017: Springer.
72. Denault, K.A., et al., *A green-yellow emitting oxyfluoride solid solution phosphor Sr₂Ba(AlO₄F)_{1-x}(SiO₅)_x:Ce³⁺ for thermally stable, high color rendition solid state white lighting*. Journal of Materials Chemistry, 2012. **22**(35): p. 18204-18213.
73. Lu, C.-H. and S. Godbole, *Synthesis and characterization of ultraviolet-emitting cerium-ion-doped SrBPO₅ phosphors*. Journal of materials research, 2004. **19**(8): p. 2336-2342.
74. Tawde, D., M. Srinivas, and K. Murthy, *Effect of lead source and cerium (III) doping on structural and photoluminescence properties of PbWO₄ microcrystallites synthesized by hydrothermal method*. physica status solidi (a), 2011. **208**(4): p. 803-807.
75. Modi, D., et al., *Hydrothermal synthesis and photoluminescence properties of cerium-doped cadmium tungstate nanophosphor*. Journal of Experimental Nanoscience, 2015. **10**(10): p. 777-786.
76. Dotsenko, V., et al., *Luminescence of Ce³⁺ ions in strontium haloborates*. Journal of luminescence, 2001. **93**(2): p. 137-145.
77. Lin, J., et al., *Does Ce⁴⁺ play a role in the luminescence of LaPO₄: Ce* Journal of Alloys and Compounds, 1995. **225**(1-2): p. 124-128.
78. Hou, D., et al., *Enhanced emission of Mn²⁺ via Ce³⁺ → Mn²⁺ energy transfer in α -Sr₂P₂O₇*. Optics Express, 2012. **20**(27): p. 28969-28980.

79. Patel, N.P., et al., *Luminescence study and dosimetry approach of Ce on an α - $\text{Sr}_2\text{P}_2\text{O}_7$ phosphor synthesized by a high-temperature combustion method*. Luminescence, 2015. **30**(4): p. 472-478.
80. Du, F., et al., *Luminescence and microstructures of Eu^{3+} -doped $\text{Ca}_9\text{LiGd}_{2/3}(\text{PO}_4)_7$* . Dalton Transactions, 2011. **40**(43): p. 11433-11440.
81. Mills, A., *Phosphors development for LED lighting*. III-Vs Review, 2005. **18**(3): p. 32-34.
82. Dubey, V., et al., *Effect of Eu^{3+} concentration on photoluminescence and thermoluminescence behavior of YBO_3 : Eu^{3+} phosphor*. Superlattices and Microstructures, 2014. **67**: p. 156-171.
83. Page, P. and K. Murthy, *Luminescence associated with Eu^{3+} in two host lattices*. Philosophical Magazine Letters, 2010. **90**(9): p. 653-662.
84. Zhang, Y., W. Gong, and G. Ning, *Novel red-emitting $\text{LiGd}(\text{WO}_4)_2$: Eu^{3+} phosphor with high thermal stability and high color purity for application in white light-emitting diodes*. New Journal of Chemistry, 2016. **40**(12): p. 10136-10143.
85. Liu, C., J. Liu, and K. Dou, *Judd–Ofelt intensity parameters and spectral properties of Gd_2O_3 : Eu^{3+} nanocrystals*. The Journal of Physical Chemistry B, 2006. **110**(41): p. 20277-20281.
86. Huang, J., et al., *Crystal structure, electronic structure, and photoluminescence properties of $\text{La}_3\text{BW}_{1-x}\text{Mo}_x\text{O}_9$: Eu^{3+} red phosphor*. Inorganic chemistry, 2014. **53**(18): p. 9541-9547.
87. Rasu, K.K., D. Balaji, and S.M. Babu, *Photoluminescence properties of Eu^{3+} : $\text{RbGd}(\text{WO}_4)_2$ red phosphors prepared by sol–gel method*. Journal of Luminescence, 2016. **170**: p. 825-834.
88. Huang, Y., et al., *The new red-emitting phosphor of oxyfluoride $\text{Ca}_2\text{RF}_4\text{PO}_4$: Eu^{3+} ($R = \text{Gd}, \text{Y}$) for solid state lighting applications*. Optics Express, 2011. **19**(7): p. 6303-6311.
89. Zhang, M., Z. Xia, and Q. Liu, *Thermally stable $\text{K}_x\text{Cs}_{1-x}\text{AlSi}_2\text{O}_6$: Eu^{2+} phosphors and their photoluminescence tuning*. Journal of Materials Chemistry C, 2017. **5**(30): p. 7489-7494.

90. Parchur, A. and R. Ningthoujam, *Behaviour of electric and magnetic dipole transitions of Eu^{3+} , Eu-O charge transfer band in Li^+ co-doped $\text{YPO}_4: \text{Eu}^{3+}$* . RSC Advances, 2012. **2**(29): p. 10859-10868.
91. Janulevicius, M., et al., *Luminescence and luminescence quenching of highly efficient $\text{Y}_2\text{Mo}_4\text{O}_{15}: \text{Eu}^{3+}$ phosphors and ceramics*. Scientific reports, 2016. **6**: p. 26098.
92. Suresh, K., et al., *Synthesis and characterization of nano Sr_2CeO_4 doped with Eu and Gd phosphor*. Journal of Luminescence, 2013. **133**: p. 96-101.
93. Ptacek, P., et al., *Crystal Phase Control of Luminescing $\alpha\text{-NaGdF}_4: \text{Eu}^{3+}$ and $\beta\text{-NaGdF}_4: \text{Eu}^{3+}$ Nanocrystals*. Advanced Functional Materials, 2007. **17**(18): p. 3843-3848.
94. Emen, F. and R. Altinkaya, *Luminescence and thermoluminescence properties of $\text{Sr}_3\text{WO}_6: \text{Eu}^{3+}$ phosphor*. Journal of Luminescence, 2013. **134**: p. 618-621.
95. Dabre, K., K. Park, and S. Dhoble, *Synthesis and photoluminescence properties of microcrystalline $\text{Sr}_2\text{ZnWO}_6: \text{RE}^{3+}$ ($\text{RE} = \text{Eu}, \text{Dy}, \text{Sm}$ and Pr) phosphors*. Journal of Alloys and Compounds, 2014. **617**: p. 129-134.
96. Zhao, X., et al., *An efficient charge compensated red phosphor $\text{Sr}_3\text{WO}_6: \text{K}^+, \text{Eu}^{3+}$ -For white LEDs*. Journal of Alloys and Compounds, 2013. **553**: p. 221-224.
97. Vishwnath, V., et al., *Synthesis and photoluminescence studies of Eu (III), Er (III) doped strontium gadolinium tantalum oxide*. Journal of fluorescence, 2016. **26**(1): p. 277-282.
98. Ayvacıklı, M., et al., *Synthesis and optical properties of Er^{3+} and Eu^{3+} doped SrAl_2O_4 phosphor ceramic*. Journal of Luminescence, 2011. **131**(11): p. 2432-2439.
99. Yadav, R., et al., *Intense red-emitting $\text{Y}_4\text{Al}_2\text{O}_9: \text{Eu}^{3+}$ phosphor with short decay time and high color purity for advanced plasma display panel*. Optics express, 2009. **17**(24): p. 22023-22030.
100. Chang, Y.-S., et al., *Synthesis and luminescent properties of Tb^{3+} -activated yttrium indium germanate phosphor*. Journal of Solid State Chemistry, 2007. **180**(11): p. 3076-3081.
101. Boruc, Z., et al., *Temperature and concentration quenching of Tb^{3+} emissions in $\text{Y}_4\text{Al}_2\text{O}_9$ crystals*. Journal of Alloys and Compounds, 2012. **532**: p. 92-97.

102. Rakov, N. and G.S. Maciel, *Energy transfer mechanism for generation of white light in Tb³⁺-doped calcium aluminosilicate amorphous powder*. Journal of Luminescence, 2017. **190**: p. 249-253.
103. Mi, R., et al., *Luminescence and energy transfer of a color tunable phosphor: Tb³⁺ and Eu³⁺ co-doped ScPO₄*. RSC Advances, 2016. **6**(34): p. 28887-28894.
104. Zhou, W., et al., *Concentration-driven selectivity of energy transfer channels and color tunability in Ba₃La(PO₄)₃: Tb³⁺, Sm³⁺ for warm white LEDs*. Inorganic chemistry, 2017. **56**(13): p. 7433-7442.
105. Kiliaan, H., J. Kotte, and G. Blasse, *Energy Transfer in the Luminescent System Na(Y,Gd)F₄: Ce, Tb*. Journal of The Electrochemical Society, 1987. **134**(9): p. 2359-2364.
106. Shang, M., et al., *Luminescence Properties of Ca₁₉Ce(PO₄)₁₄: A (A= Eu³⁺, Tb³⁺, Mn²⁺) Phosphors with Abundant Colors: Abnormal Coexistence of Ce^{4+/3+}-Eu³⁺ and Energy Transfer of Ce³⁺→ Tb³⁺/Mn²⁺ and Tb³⁺-Mn²⁺*. Inorganic chemistry, 2017. **56**(11): p. 6131-6140.
107. Zambare, A. and K. Murthy, *Photoluminescence studies of Eu doped Yttrium based phosphors*. Archives of Physics Research, 2011. **2**(3): p. 46-50.
108. Murthy, K., A.S. Prasad, and M.R. Rao, *Luminescence characteristics of Eu and Tb doped YGdBO₃ phosphor*. Physics Procedia, 2012. **29**: p. 70-75.
109. Xia, Z. and R.-S. Liu, *Tunable blue-green color emission and energy transfer of Ca₂Al₃O₆F: Ce³⁺, Tb³⁺ phosphors for near-UV white LEDs*. The Journal of Physical Chemistry C, 2012. **116**(29): p. 15604-15609.
110. Lai, H., et al., *UV Luminescence Property of YPO₄: RE (RE= Ce³⁺, Tb³⁺)*. The Journal of Physical Chemistry C, 2008. **112**(1): p. 282-286.
111. Chaudhari, K., et al., *Effect of RE Dopant (Ce & Tb) on PL and Crystallites size of Lanthanum Phosphor (LaPO₄)*. Adv Appl Sci Res, 2011. **2**: p. 130-135.
112. Nair, G.B. and S. Dhoble, *Highly enterprising calcium zirconium phosphate [CaZr₄(PO₄)₆: Dy³⁺, Ce³⁺] phosphor for white light emission*. RSC Advances, 2015. **5**(61): p. 49235-49247.
113. Xu, M., et al., *Enhancing the luminescent properities of Zn₂P₂O₇: Ce³⁺, Dy³⁺ via efficient energy transfer*. Materials Research Bulletin, 2015. **70**: p. 691-696.